International Geology Review, 2015
Vol. 57, No. 3, 373–392, http://dx.doi.org/10.1080/00206814.2015.1009503

Taylor & Francis
Taylor & Francis Group

Zircon U–Pb geochronology and geochemistry of Late Cretaceous–early Eocene granodiorites in the southern Gangdese batholith of Tibet: petrogenesis and implications for geodynamics and Cu ± Au ± Mo mineralization

Ziqi Jiang[a,b,c], Qiang Wang[a]*, Derek A. Wyman[d], Xiaobin Shi[c], Jinhui Yang[e], Lin Ma[a] and Guoning Gou[a]

[a]*State Key Laboratory of Isotope Geochemistry, Guangzhou Institute of Geochemistry, Chinese Academy of Sciences, Guangzhou, China;* [b]*School of Earth Science, Guilin University of Technology, Guilin, China;* [c]*Key Laboratory of Marginal Sea Geology, South China Sea Institute of Oceanology, Chinese Academy of Sciences, Guangzhou, China;* [d]*School of Geosciences, The University of Sydney, Sydney, Australia;* [e]*State Key Laboratory of Lithosphere Evolution, Institute of Geology and Geophysics, Chinese Academy of Science, Beijing, China*

(*Received 8 July 2014; accepted 14 January 2015*)

Cu ± Au ± Mo mineralization is found in multiple intrusive suites in the Gangdese belt of southern Tibet (GBST). However, the petrogenesis of these ore-bearing intrusive rocks remains controversial. Here, we report on mineralization-related Late Cretaceous-early Eocene intrusive rocks in the Chikang–Jirong area, southern Gangdese. Zircon U–Pb analyses indicate that the mainly granodioritic Chikang and Jirong plutons were generated in the Late Cretaceous (ca. 92 Ma) and early Eocene (ca. 53 Ma), respectively. They are high-K calc-alkaline suites with high SiO_2 (64.8–68.3 wt.%) and Al_2O_3 (15.1–15.7 wt.%) contents. Chikang granodiorites are characterized by high Sr (835–957 ppm), Sr/Y (118–140), Mg# (58–60), Cr (21.8–36.6 ppm), and Ni (14.3–22.9 ppm), and low Y (6.0–8.1 ppm), Yb (0.54–0.68 ppm) values with negligible Eu anomalies, which are similar to those of typical slab-derived adakites. The Jirong granodiorites have high SiO_2 (64.8–65.3 wt.%) and $Na_2O + K_2O$ (7.19–7.59 wt.%), and low CaO (2.45–3.69 wt.%) contents, Mg# (47–53) and Sr/Y (14–16) values, along with negative Eu and Ba anomalies. Both Chikang and Jirong granodiorites have similar $\varepsilon_{Hf}(t)$ (7.6–13.1) values. The Chikang granodiorites were most probably produced by partial melting of subducted Neo-Tethyan oceanic crust, and the Jirong granodiorites were possibly generated by partial melting of Gangdese juvenile basaltic crust. In combination with the two peak ages (100–80 and 65–41 Ma) of Gangdese magmatism, we suggest that upwelling asthenosphere, triggered by the rollback and subsequent break-off of subducted Neo-Tethyan oceanic lithosphere, provided the heat for partial melting of subducted slab and arc juvenile crust. Taking into account the contemporaneous occurrence of Gangdese magmatism and Cu ± Au ± Mo mineralization, we conclude that the Late Cretaceous–early Eocene magmatic rocks in the GBST may have a significant potential for Cu ± Au ± Mo mineralization.

Keywords: adakitic rocks; slab melting; slab rollback; slab break-off; Cu ± Au ± Mo mineralization; Gangdese belt

1. Introduction

Porphyry Cu ± Au ± Mo deposits often occur in subduction-related arc (Cooke *et al.* 2005; Sillitoe 2010) or post-collisional orogenic (Hou *et al.* 2004, 2009, 2013) settings worldwide. In recent years, numerous Miocene (18–13 Ma) porphyry Cu ± Au ± Mo deposits have been discovered in the Gangdese belt of southern Tibet (GBST) (Chung *et al.* 2003; Hou *et al.* 2004, 2013; Leng *et al.* 2013), which are closely associated with post-collisional adakitic rocks (Hou *et al.* 2004, 2013; Qu *et al.* 2004). Several older arc and collision-related porphyry-/skarn-type Cu ± Au ± Mo deposits have also been recognized in the GBST (Figure 1c), such as the Middle Jurassic Xiongcun porphyry Cu–Au deposit (ca. 182–160 Ma, Tafti *et al.* 2009; Lang *et al.* 2014), the Late Cretaceous Kelu (ca. 93–90 Ma, Jiang *et al.* 2012) and Sambujiala skarn Cu–Au deposits (ca. 94–92 Ma, Liang *et al.* 2010; Zhao *et al.* 2013), and the Eocene Jiru porphyry Cu–Mo (51–45 Ma, Zhang *et al.* 2008; Zheng *et al.* 2014b), Sharang porphyry Mo (53–51 Ma, Zhao *et al.* 2014), Jiaduobule skarn Fe–Cu (ca. 51 Ma, Yu *et al.* 2011a), and Lamda skarn Cu deposits (48 Ma, Zhang *et al.* 2008). These data define three epochs (Middle Jurassic (182–160 Ma), Late Cretaceous (ca. 90 Ma) and early Eocene (ca. 50 Ma)) for Cu ± Au ± Mo mineralization in the region.

Detailed geochronological data show that there are two intense magmatic peaks (100–80 Ma and 65–41 Ma) in the GBST (Wen *et al.* 2008b; Ji *et al.* 2009b; Ma *et al.* 2013a), meaning that the Late Cretaceous (~90 Ma) and early Eocene (~50 Ma) Cu ± Au ± Mo mineralization events coincide with the mid-points of these peaks. However, the geodynamic context for these two periods of magmatism and mineralization remains highly controversial. For example, various trigger mechanisms have been proposed for the Late Cretaceous (ca. 100–80 Ma) magmatism, such

*Corresponding author. Email: wqiang@gig.ac.cn

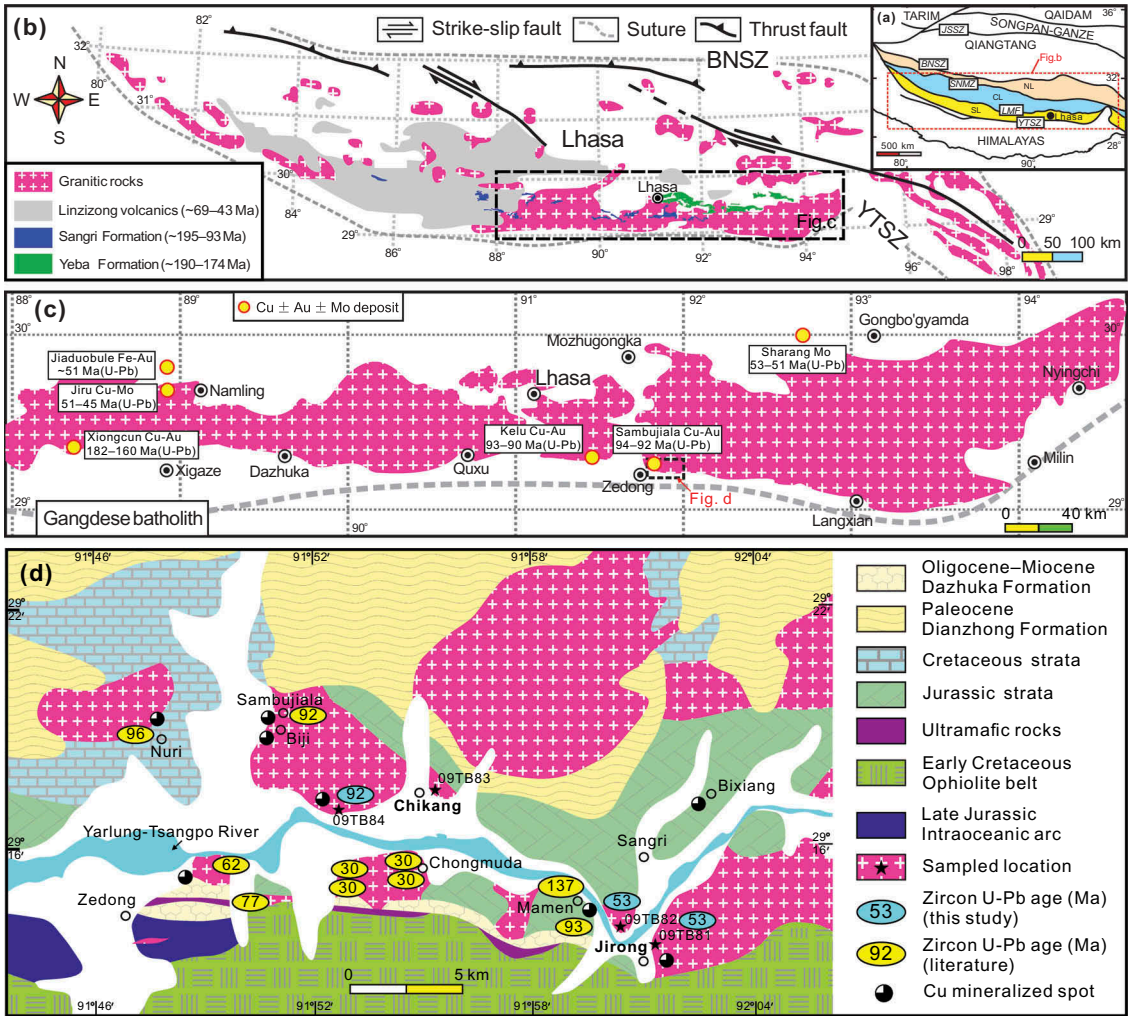

Figure 1. (a) Diagram showing the Lhasa block in the context of the Tibetan Plateau (modified from Zhu *et al.* 2011). The age data for the Linzizong volcanic rocks are from Lee *et al.* (2009). The age data for the volcanic rocks of the Sangri Formation are from Kang *et al.* (2010) and Kang *et al.* 2014. The age data for the volcanic rocks of the Yeba Formation are from Zhu *et al.* (2008). Abbreviations: TARIM, Tarim craton; QAIDAM, Qaidam block; JSSZ, Jinsha suture zone; BNSZ, Bangong–Nujiang suture zone; SNMZ, Shiquan River–Nam Tso Mélange zone; LMF, Luobadui–Milashan Fault; YTSZ, Yarlung–Tsangpo suture zone; SL, Southern Lhasa block; CL, Central Lhasa block; NL, Northern Lhasa block. (b) Geological map of the Lhasa block (modified from Ma *et al.* 2013c). Abbreviations: BNSZ, Bangong–Nujiang suture zone; YTSZ, Yarlung–Tsangpo suture zone; Lhasa, Lhasa block. (c) Distribution map of Late Cretaceous–Eocene Cu ± Au ± Mo deposits in the Gangdese belt (modified after Ma *et al.* 2013c). The location and emplacement age of Late Cretaceous–Eocene Cu ± Au ± Mo deposits were collected from these references (Zhang *et al.* 2008; Tafti *et al.* 2009; Yu *et al.* 2011a; Jiang *et al.* 2012; Zhao *et al.* 2013, 2014; Lang *et al.* 2014; Zheng *et al.* 2014b). The Jiru Cu–Mo mineralization is mainly associated with Eocene Jiru monzogranite (Zheng *et al.*, 2014b). The location of the Jiru Cu–Mo mineralization is the same as that of the Jiru monzogranite. (d) Geological map of study area (modified after Ma *et al.* 2013b), showing the sampling locations and ages. The locations of samples 09TB81 and 09TB82, and 09TB83 and 09TB84 represent those of the Jirong and Chikang plutons, respectively. The zircon U–Pb age data are from Zhu *et al.* (2009), Liang *et al.* (2010), Jiang *et al.* (2014), and Zheng *et al.* (2014a). The Cu mineralized spot locations are after Chen *et al.* (2012).

as low-angle or flat oceanic slab subduction (Wen *et al.* 2008a, 2008b), oceanic ridge subduction (Zhang *et al.* 2010a; Zheng *et al.* 2014a), and rollback of subducted oceanic slab (DeCelles *et al.* 2007; Ma *et al.* 2013a, 2013b, 2013c; Chen *et al.* 2015; Jiang *et al.* 2014). Similarly, both Neo-Tethyan oceanic slab rollback (Zhao *et al.* 2014) and slab break-off (Ma *et al.* 2014; Jiang *et al.* 2014; Zheng *et al.* 2014b; Chen *et al.* 2015) have been proposed to account for the 65–41 Ma magmatism and related Cu ± Au ± Mo mineralization.

In this study, we present new geochemical and zircon U–Pb ages and *in situ* Lu–Hf isotopic data for Late Cretaceous–early Eocene intrusive rocks associated with Cu ± Au ± Mo mineralization in the Chikang–Jirong area, southern GBST. These new data, together with previously published data, provide important evidence for the

petrogenesis and geodynamic processes responsible for generating both magmatism and Cu ± Au ± Mo mineralization in the GBST.

2. Geological background and rock characteristics

From south to north, the Tibetan Plateau consists of the Himalaya, Lhasa, Qiangtang, Songpan–Ganze, and Kunlun–Qaidam blocks (Figure 1a) (Yin and Harrison 2000). The Lhasa block, located in the southern part of Tibet Plateau, is between the Yarlung–Tsangpo suture (YTS) to the south and the Bangong–Nujiang suture (BNS) to the north (Figure 1b) (Yin and Harrison 2000). The YTS marks the closure of the Neo-Tethyan ocean during India–Asia collision (65–50 Ma) (Najman *et al.* 2010; Wu *et al.* 2014; Jiang *et al.* 2014). The Lhasa block can be further divided into the northern, central, and southern subblocks, separated by the Shiquan River–Nam Tso Melange zone (SNMZ) and Luobadui–Milashan Fault (LMF), respectively (Figure 1a) (Zhu *et al.* 2011, 2013).

The GBST is dominated by juvenile crust but includes minor Precambrian basement and represents a Phanerozoic subduction-related Andean-style accretionary convergent margin related to the northward subduction of Neo-Tethyan oceanic lithosphere prior to India colliding with Asia along the YTS (Figure 1b) (Yin and Harrison 2000; Zhu *et al.* 2011). Voluminous Cretaceous–Eocene calc-alkaline granitoids (the main part of Gangdese batholith) and Late Jurassic–early Tertiary volcanic sequences (e.g. Yeba, Sangri and Linzizong volcanic successions) occur along the 1600 km-long E–W-trending Gangdese magmatic belt of the southern Lhasa block (Figure 1b) (Wen *et al.* 2008b; Ji *et al.* 2009b; Wu *et al.* 2010). Abundant zircon U–Pb and whole-rock $^{40}Ar/^{39}Ar$ data for the igneous and volcanic rocks emplaced in the GBST delineate two episodes of intense magmatic activity, including the Late Cretaceous (ca. 106–80 Ma), dominated by voluminous slab-derived adakitic rocks (Wen *et al.* 2008b; Ji *et al.* 2009b; Zhang *et al.* 2010a; Jiang *et al.* 2012; Ma *et al.* 2013a, 2013c; Chen *et al.* 2015), and early Tertiary (65–41 Ma) basaltic to rhyolitic lavas and intrusive rocks (Mo *et al.* 2007, 2008; Wen *et al.* 2008b; Lee *et al.* 2009, 2012; Ji *et al.* 2009b; Ma *et al.* 2014; Jiang *et al.* 2014; Chen *et al.* 2015).

The Chikang–Jirong area in the southern GBST is adjacent to the YTS (Figure 1d). Magmatic rocks in the Chikang–Jirong area were mainly generated during Jurassic to Oligocene time (137–30 Ma) (Zhu *et al.* 2009; Liang *et al.* 2010; Jiang *et al.* 2014; Zheng *et al.* 2014a). Two plutons in the Chikang–Jirong area were investigated in this study (Figure 1d). The Jirong and Chikang plutons mainly consist of granodiorite (Figure 2), which intrudes Jurassic sediments and is overlain by Quaternary sediments. To the northwest of the Chikang pluton, a skarn-type Cu deposit has been discovered in the Sumbajiala area (Figure 1d), where the copper

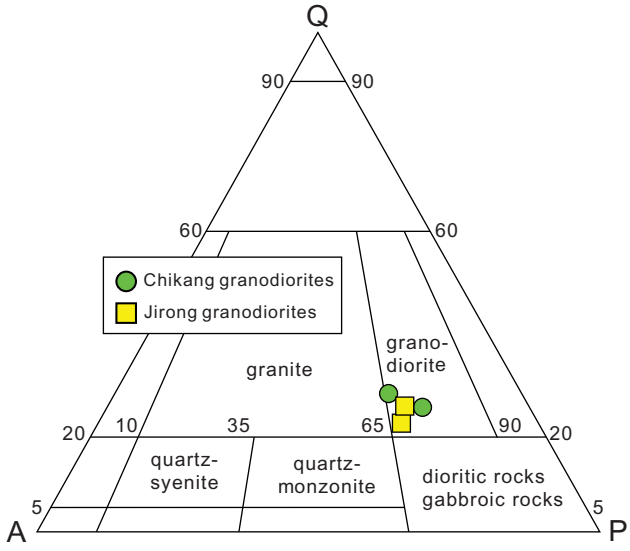

Figure 2. QAP (Streckeisen 1976) diagram for Jirong–Chikang intrusive rocks. Q, modal quartz; A, modal alkali feldspar; P, modal plagioclase.

mineralization is predominantly hosted by granodiorite. Laser ablation inductively coupled plasma mass spectrometry (LA-ICP-MS) zircon U–Pb dating of the host granodiorites yielded an age of 92.1 ± 0.6 Ma (Liang *et al.* 2010). The Jirong granodiorites have fine-grained texture and massive structure and are composed of plagioclase (~40–45 vol.%), subhedral K-feldspar (~20–25 vol.%), quartz (~10–15 vol.%), hornblende (~5–10 vol.%), and biotite (~5–8 vol.%) with minor zircon, apatite, and magnetite (Figure 3a). The Chikang granodiorites exhibit medium-grained textures and massive structure and consist of plagioclase (~40–45 vol.%), K-feldspar (~20–25 vol.%), quartz (~12–15 vol.%), hornblende (~5–10 vol.%), and biotite (~5–10 vol.%) with minor zircon, apatite, and magnetite (Figure 3b).

3. Analytical methods

Zircons were separated using conventional heavy-liquid and magnetic separation techniques at the Langfang Mineral Separation Laboratory, near Beijing. Zircon grains were hand-picked and mounted in an epoxy resin disc, and then polished and coated with gold. Cathodoluminescence (CL) images were taken at the State Key Laboratory of Isotope Geochemistry, Guangzhou Institute of Geochemistry, Chinese Academy of Sciences (SKLaBIG GIG CAS), with a JEOL JXA-8100 Superprobe for inspecting internal morphology of individual zircons and for selecting positions for U–Pb, Lu–Hf isotope analyses.

Zircon U–Pb dating was conducted at the multi-collector (MC)-ICPMS laboratory of the Institute of Geology and Geophysics, Chinese Academy of Sciences

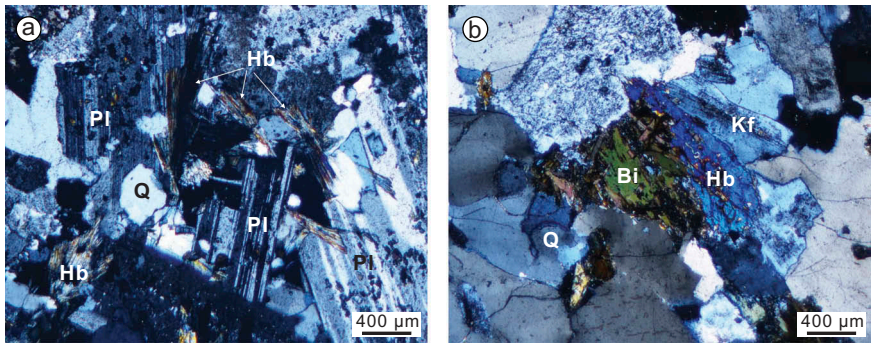

Figure 3. Petrography of the Jirong–Chikang intrusive rocks: (a) Jirong granodiorites, hornblendes have been subjected to variable degrees of alteration; (b) Chikang granodiorites. Abbreviations: Pl, plagioclase; Q, quartz; Bi, biotite; Hb, hornblende; Kf, potassic feldspar.

(IGG CAS) in Beijing. Detailed operating conditions for the laser ablation system and the ICP-MS instrument and data reduction were the same as described by Xie *et al.* (2008). An Agilent 7500a quadruple (Q)-ICPMS and a Neptune (MC)-ICPMS with a 193 nm excimer ArF laser-ablation system (GeoLas Plus) attached were used for simultaneous determination of zircon U–Pb ages. A suite of zircon standards, that is Harvard zircon 91,500 (Wiedenbeck *et al.* 1995), Australian Macquarie University standard zircon GJ–1 (Jackson *et al.* 2004), and NIST SRM 610, were analysed following each five samples. Every spot analysis consisted of approximately 30 s background acquisition and 40 s sample data acquisition. $^{207}Pb/^{206}Pb$, $^{206}Pb/^{238}U$, $^{207}U/^{235}U$ ($^{235}U = {}^{238}U/137.88$), and $^{208}Pb/^{232}Th$ ratios were corrected by using zircon 91,500 as the external standard. The fractionation correction and results were calculated using GLITTER 4.0 (Macquarie University) (Jackson *et al.* 2004). Common Pb was corrected according to the method of Andersen (2002). The weighted mean U–Pb ages and concordia plots were processed using ISOPLOT 3.0 (Ludwig 2003). *In situ* Hf isotope measurements were subsequently done using LA-ICPMS with a beam size of 60 μm and laser pulse frequency of 8 Hz with age determinations at the MC-ICPMS laboratory of IGG CAS. Details of instrumental conditions and data acquisition are given in Wu *et al.* (2006). The isobaric interference of ^{176}Lu on ^{176}Hf is negligible due to the extremely low $^{176}Lu/^{177}Hf$ in zircon (normally < 0.002). During the analyses for this study, GJ-1 analysed as an unknown yielded a weighted $^{206}Pb/^{238}U$ age of 609.7 ± 6.3 Ma ($2\sigma_n$, mean standard weighted deviation (MSWD) = 0.97, n = 12) and a weighted $^{176}Hf/^{177}Hf$ ratio of 0.282015 ± 0.000003 ($2\sigma_n$, MSWD = 1.12, n = 94), which is in good agreement with the recommended U–Pb age and Hf isotopic ratio (Wu *et al.* 2006).

Rock samples were examined by optical microscopy, and selected whole-rock samples were sawed into small chips and ultrasonically cleaned in distilled water with <3% HNO_3 and then in distilled water alone and subsequently dried and hand-picked to remove visible alteration. The rocks were powdered in a chrome ring mill, and the resulting powders were used for analyses of major and trace elements at SKLaBIG GIG CAS. Major-element oxides were analysed using a Rigaku RIX 2000 X-ray fluorescence spectrometer at SKLaBIG GIG CAS on fused glass beads. Calibration lines used in quantification were produced by bivariate regression of data from 36 reference materials encompassing a wide range of silica compositions (Li *et al.* 2005), and analytical uncertainties are between 1% and 5%. Trace elements were analysed by ICP-MS, using a Perkin-Elmer Sciex ELAN 6000 instrument at SKLaBIG GIG CAS. Analytical procedures are the same as those described by Li *et al.* (2002). Repeated runs give <5% relative standard deviation (RSD) for most elements of reference materials analysed by ICP-MS.

4. Analytical results

4.1. Zircon U–Pb geochronology

The results of zircon LA-ICPMS U–Pb isotopic analyses for the Chikang and Jirong intrusive rocks are given in Table 1. U–Pb concordia plots and representative CL images of zircons are shown in Figure 4. Most zircon grains are colourless, transparent and show euhedral prismatic forms (70–200 μm). Zircon crystals display oscillatory zoning (Figure 4), typical of a magmatic origin (Corfu *et al.* 2003). All of the analysed zircons have variable Th (94–671 ppm) and U (152–655 ppm) contents with Th/U ratios ranging from 0.51 to 1.17 (Table 1), indicating a magmatic origin for these zircons (Hoskin and Schaltegger 2003). Zircons from two samples (09TB81 and 09TB82) of the Jirong granodiorites yielded consistent $^{206}Pb/^{238}U$ ages, with the coincident weighted mean ages of 53.2 ± 0.6 Ma (Figure 4a) and 53.2 ± 0.7 Ma (Figure 4b), respectively. Ten analyses of Chikang granodiorites (09TB84) yielded $^{206}Pb/^{238}U$ ages of 91–92 Ma, with a weighted mean age of 91.8 ± 1.3 Ma (Figure 4c).

Table 1. LA-ICP-MS zircon U–Pb data of the Chikang and Jirong pluton.

Analysis	Content (ppm)			Isotopic ratios						Isotopic ages (Ma)					
	Th	U	Th/U	$^{207}Pb/^{206}Pb$	±1σ	$^{207}Pb/^{235}U$	±1σ	$^{206}Pb/^{238}U$	±1σ	$^{207}Pb/^{206}Pb$	±1σ	$^{207}Pb/^{235}U$	±1σ	$^{206}Pb/^{238}U$	±1σ
09TB81 Jirong granodiorite															
09TB81 01	165	243	0.68	0.0520	0.0027	0.0593	0.0032	0.0083	0.0002	284	89	59.0	3.0	53.5	1.0
09TB81 02	127	215	0.59	0.0503	0.0036	0.0575	0.0040	0.0083	0.0002	209	165	57.0	4.0	53.2	0.9
09TB81 03	124	213	0.58	0.0491	0.0026	0.0539	0.0026	0.0083	0.0001	151	81	53.0	2.0	53.4	0.9
09TB81 04	190	292	0.65	0.0506	0.0022	0.0573	0.0025	0.0083	0.0001	224	68	57.0	2.0	53.5	0.9
09TB81 05	465	655	0.71	0.0483	0.0014	0.0554	0.0017	0.0083	0.0001	116	47	55.0	2.0	53.5	0.7
09TB81 06	125	215	0.58	0.0528	0.0029	0.0592	0.0031	0.0083	0.0002	320	80	58.0	3.0	53.0	1.0
09TB81 07	94	183	0.51	0.0464	0.0031	0.0528	0.0035	0.0083	0.0001	20	149	52.0	3.0	52.9	0.9
09TB81 08	128	238	0.54	0.0464	0.0031	0.0530	0.0034	0.0083	0.0002	19	149	52.0	3.0	53.0	1.0
09TB81 09	671	575	1.17	0.0461	0.0018	0.0524	0.0019	0.0083	0.0001		80	52.0	2.0	53.0	0.8
09TB81 10	139	223	0.62	0.0536	0.0039	0.0583	0.0037	0.0083	0.0002	352	100	58.0	4.0	53.0	1.0
09TB81 11	467	586	0.80	0.0483	0.0022	0.0540	0.0022	0.0083	0.0002	115	51	53.0	2.0	53.0	1.0
09TB82 Jirong granodiorite															
09TB82 01	130	179	0.72	0.0464	0.0042	0.0529	0.0047	0.0083	0.0002	20	198	52.0	4.0	53.0	1.0
09TB82 02	103	152	0.68	0.0588	0.0034	0.0646	0.0035	0.0083	0.0002	561	79	64.0	3.0	54.0	1.0
09TB82 03	137	178	0.77	0.0579	0.0054	0.0609	0.0043	0.0083	0.0002	526	124	60.0	4.0	53.4	1.0
09TB82 04	115	154	0.75	0.0547	0.0049	0.0599	0.0050	0.0083	0.0002	400	140	59.0	5.0	53.0	1.0
09TB82 05	146	227	0.64	0.0484	0.0027	0.0535	0.0029	0.0083	0.0002	120	85	53.0	3.0	53.0	1.0
09TB82 06	115	185	0.62	0.0461	0.0055	0.0520	0.0059	0.0082	0.0003	1	236	51.0	6.0	53.0	2.0
09TB82 07	132	172	0.77	0.0481	0.0045	0.0548	0.0050	0.0083	0.0002	105	209	54.0	5.0	53.0	1.0
09TB82 08	171	179	0.95	0.0479	0.0040	0.0534	0.0041	0.0083	0.0002	95	126	53.0	4.0	53.0	1.0
09TB82 09	139	185	0.75	0.0516	0.0067	0.0569	0.0066	0.0084	0.0003	268	200	56.0	6.0	54.0	2.0
09TB82 10	208	236	0.88	0.0507	0.0042	0.0537	0.0036	0.0083	0.0002	227	106	53.0	3.0	53.0	1.0
09TB82 11	150	204	0.73	0.0487	0.0032	0.0555	0.0038	0.0083	0.0002	134	113	55.0	4.0	53.0	1.0
09TB82 12	148	208	0.71	0.0515	0.0048	0.0585	0.0058	0.0083	0.0002	263	168	58.0	6.0	53.0	2.0
09TB84 Chikang granodiorite															
09TB84 01	346	432	0.80	0.0566	0.0027	0.1119	0.0061	0.0144	0.0003	476	81	108.0	6.0	92.0	2.0
09TB84 02	325	422	0.77	0.0483	0.0030	0.0949	0.0055	0.0144	0.0003	113	92	92.0	5.0	92.0	2.0
09TB84 03	206	268	0.77	0.0479	0.0019	0.0950	0.0060	0.0144	0.0002	94	113	92.0	6.0	92.0	1.0
09TB84 04	289	318	0.91	0.0461	0.0027	0.0905	0.0051	0.0143	0.0002		128	88.0	5.0	91.0	1.0
09TB84 05	283	329	0.86	0.0514	0.0043	0.1024	0.0100	0.0144	0.0004	260	165	99.0	9.0	92.0	3.0
09TB84 06	177	233	0.76	0.0511	0.0028	0.0981	0.0062	0.0144	0.0003	244	101	95.0	6.0	92.0	2.0
09TB84 07	286	358	0.80	0.0512	0.0019	0.1007	0.0046	0.0144	0.0002	249	82	97.0	4.0	92.0	1.0
09TB84 08	384	447	0.86	0.0510	0.0027	0.1018	0.0063	0.0144	0.0002	239	115	98.0	6.0	92.0	1.0
09TB84 09	215	303	0.71	0.0542	0.0032	0.1059	0.0064	0.0144	0.0003	380	97	102.0	6.0	92.0	2.0
09TB84 10	260	388	0.67	0.0499	0.0017	0.0954	0.0034	0.0145	0.0004	188	38	93.0	3.0	92.0	3.0

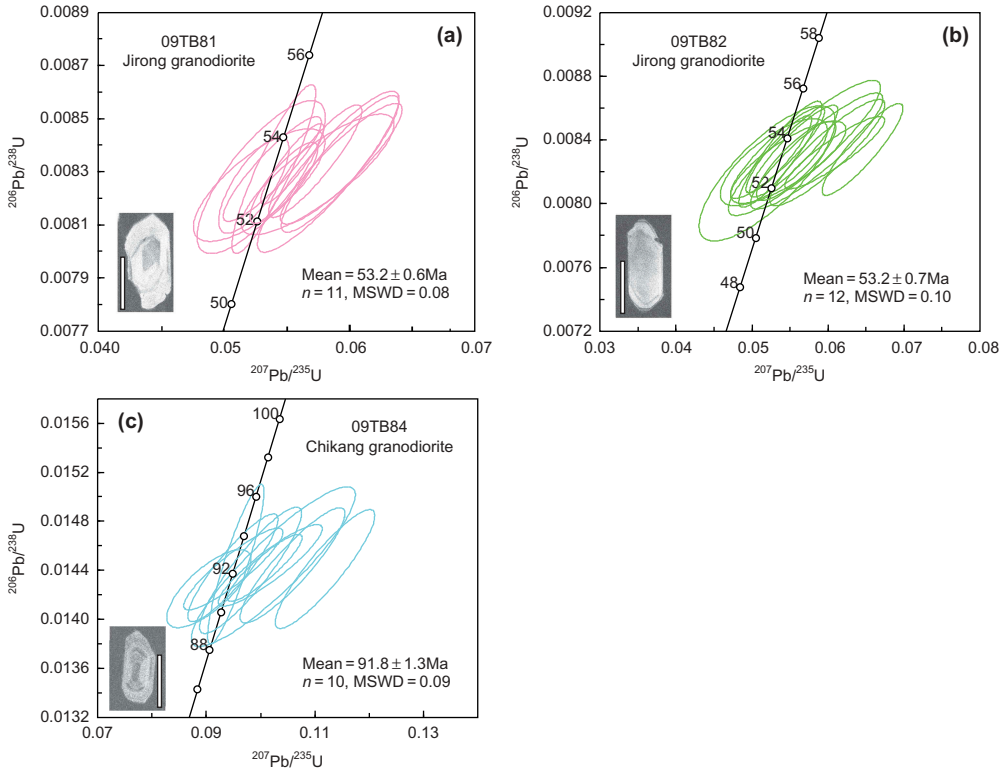

Figure 4. LA-ICP-MS zircon U–Pb Concordia diagrams for the Jirong granodiorites (a–b) and Chikang granodiorites (c) in southern Tibet. White bars in the zircon CL images represent 100 μm.

4.2. *Whole-rock major and trace elements*

Whole-rock major and trace element data of the Jirong and Chikang granodiorites are presented in Table 2. On the SiO_2 vs. $K_2O + Na_2O$ diagram (Figure 5a), all samples plot in the granodiorite field, except for one Jirong pluton sample in the quartz monzonite field. They have high SiO_2 (64.84–68.29 wt.%), Al_2O_3 (15.05–15.67 wt.%), K_2O (3.14–3.97 wt.%), and Na_2O (3.72–4.05 wt.%) contents with K_2O/Na_2O = 0.77–1.10. All samples are high-K calc-alkaline (Figure 5b) and metaluminous to slightly peraluminous (A/CNK = 0.89–1.08) (Figure 5c). The Jirong granodiorites have low Mg# (47–53), Sr (232–284 ppm), Cr (5.57–17.1 ppm), and Ni (5.68–10.2 ppm) and Sr/Y (14–16) values (Table 2). Compared with the Jirong granodiorites, the Chikang granodiorites have high Sr (835–957 ppm), Sr/Y (118–140), Mg# (58–60), Cr (21.8–36.6 ppm), and Ni (14.3–22.9 ppm), and low Y (6.0–8.1 ppm) and Yb (0.54–0.68 ppm) values (Figure 5d–f, Table 2), similar to those of typical slab-derived adakitic rocks (Defant and Drummond 1990; Zhu *et al.* 2009; Jiang *et al.* 2012, 2014; Ma *et al.* 2013c).

On chondrite-normalized rare earth element (REE) patterns (Figure 6a and b), they exhibit light rare earth element (LREE) enrichment and heavy rare earth element (HREE) depletion. The Jirong granodiorites have moderate negative Eu anomalies and slightly higher HREE contents than the Chikang granodiorites (e.g. Yb = 1.61–2.04 ppm, Y = 14.8–19.7 ppm). The Chikang granodiorites have negligible Eu anomalies. The primitive mantle-normalized trace-element distribution patterns of both suites (Figure 6c and d) are characterized by the relative enrichment of large ion lithophile elements (LILEs) and depletion of high field strength elements (HFSEs). All the samples exhibit significant negative Ta–Nb–Ti anomalies.

4.3. *Zircon Lu-Hf isotope geochemistry*

The zircon Hf isotopic compositions of the Chikang–Jirong granodiorites are given in Table 3, and further illustrated in Figure 8. The Chikang granodiorites have high $\varepsilon_{Hf}(t)$ (8.5–13.1) values similar to those of the Jirong granodiorites (7.6–10.4). They have similar T_{DM}^{C} values ranging from 316 to 639 Ma. The Chikang and Jirong granodiorites have $\varepsilon_{Hf}(t)$ values similar to those of Gangdese belt Late Cretaceous slab-derived adakitic rocks (Jiang *et al.* 2012; Ma *et al.* 2013c) and Palaeogene–Eocene granotoids (Guan *et al.* 2012; Jiang *et al.* 2014) exposed in the GBST (Figure 8), respectively.

Table 2. Major (wt.%) and trace (ppm) data for the Chikang and Jirong pluton.

Locality	Jirong		Chikang		Sambujiala*					
Sample	09TB81	09TB82	09TB83	09TB84	B003-2	B004-1	B007-2	B008-1	B009-1	B028-2
Longitude	92°01′23″	92°00′27″	91°55′10″	91°52′38″						
Latitude	29°14′57″	29°14′07″	29°17′29″	29°16′52″						
Classify	Granodiorite				Granodiorite					
Age	53	53		92						
SiO_2	64.84	65.28	68.29	66.82	66.02	65.77	65.1	64.42	64.05	62.24
TiO_2	0.52	0.59	0.39	0.49	0.53	0.49	0.54	0.56	0.51	0.57
Al_2O_3	15.67	15.05	15.28	15.26	15.1	15.11	15.46	15.25	15.09	15.21
$Fe_2O_3^T$	4.07	4.00	2.61	3.29						
Fe_2O_3					0.23	1.48	2.29	0.95	1.37	1.76
FeO					3.07	2.03	1.51	3.02	2.26	2.44
MnO	0.06	0.05	0.04	0.05	0.05	0.05	0.08	0.08	0.07	0.08
MgO	1.57	1.92	1.52	2.11	2.11	2.02	2.16	2.47	2.27	2.38
CaO	2.45	3.69	2.83	3.56	3.98	3.74	4.17	4.37	4.32	4.78
Na_2O	4.05	3.62	3.72	3.72	3.5	3.52	3.65	3.5	3.94	3.96
K_2O	3.14	3.97	3.68	3.53	3.32	3.26	2.94	2.82	2.75	2.74
P_2O_5	0.11	0.12	0.15	0.18	0.21	0.2	0.09	0.23	0.22	0.25
L.O.I	3.33	1.48	1.24	0.76	2.08	2.58	1.29	2.42	2.65	3.02
Total	99.81	99.75	99.76	99.76						
$Mg^{\#}$	47	53	58	60	51	56	49	58	55	64
Sc	8.61	9.56	5.18	7.00	9.95	10.2	8.01	10.7	8.87	9.35
V	83.0	90.5	64.1	84.7						
Cr	5.57	17.1	21.8	36.6						
Co	32.8	47.7	60.9	52.8						
Ni	5.68	10.2	14.3	22.9						
Ga	15.6	15.4	15.3	16.4						
Ge	1.26	1.22	1.13	1.17						
Rb	12.0	138	98.1	84.9	96.3	84.2	76.2	84.6	79.0	65.7
Sr	232	284	835	957	802	841	1100	939	1076	1547
Y	14.8	19.7	5.96	8.06	9.02	9.68	9.93	10.7	10.2	11.7
Zr	137	134	113	92.0	95.8	95.0	80.8	141	81.5	89.2
Nb	5.87	7.65	4.53	5.27	4.01	4.57	4.79	4.48	3.98	4.73
Cs	10.8	2.86	2.50	2.21						
Ba	475	448	571	767	384	465	405	481	575	493
La	22.2	25.3	23.9	28.3	23.7	23.7	24.9	24.9	24.2	25.6
Ce	42.1	49.4	41.3	52.4	46.8	48.2	45.3	49.3	44.0	48.8
Pr	4.94	6.01	4.54	6.07	5.43	5.58	5.31	5.81	5.07	5.90
Nd	17.5	21.7	15.6	21.6	21.3	21.1	20.3	22.2	19.5	22.8
Sm	3.18	4.12	2.39	3.38	3.49	3.61	3.34	3.60	3.35	3.89
Eu	0.750	0.830	0.750	1.01	1.04	0.980	0.960	1.02	0.910	0.980
Gd	2.77	3.65	1.76	2.61	2.53	2.80	2.85	2.84	2.82	3.18

(*Continued*)

Table 2. (Continued).

Locality	Jirong		Chikang		Sambujiala*					
Sample	09TB81	09TB82	09TB83	09TB84	B003-2	B004-1	B007-2	B008-1	B009-1	B028-2
Tb	0.442	0.591	0.225	0.331	0.390	0.400	0.360	0.440	0.340	0.400
Dy	2.57	3.38	1.06	1.55	2.01	1.98	1.89	2.14	1.90	2.20
Ho	0.517	0.688	0.193	0.281	0.390	0.400	0.360	0.450	0.360	0.410
Er	1.50	1.97	0.516	0.732	1.09	1.09	0.980	1.28	1.01	1.14
Tm	0.234	0.293	0.083	0.105	0.160	0.150	0.170	0.180	0.150	0.180
Yb	1.61	2.04	0.537	0.676	1.05	1.13	1.04	1.24	1.05	1.24
Lu	0.250	0.308	0.0860	0.106	0.160	0.170	0.160	0.180	0.170	0.170
Hf	3.80	3.92	2.82	2.52	3.10	2.92	2.72	4.29	2.62	2.82
Ta	0.640	0.936	0.550	0.565	0.340	0.430	0.580	0.410	0.370	0.530
Pb	14.2	8.01	8.33	10.2	11.3	11.5	13.3	7.61	6.58	9.11
Th	11.7	17.4	8.60	7.82	7.82	7.59	9.62	8.85	7.71	7.47
U	3.32	4.40	1.95	2.51	2.29	1.73	2.64	2.06	3.27	1.58

Notes: *Published data from Zhao *et al.* (2013).
Mg# = 100 × molar $Mg^{2+}/(Mg^{2+} + Fe^{2+})$, assuming $FeO/(FeO + Fe_2O_3) = 0.85$.

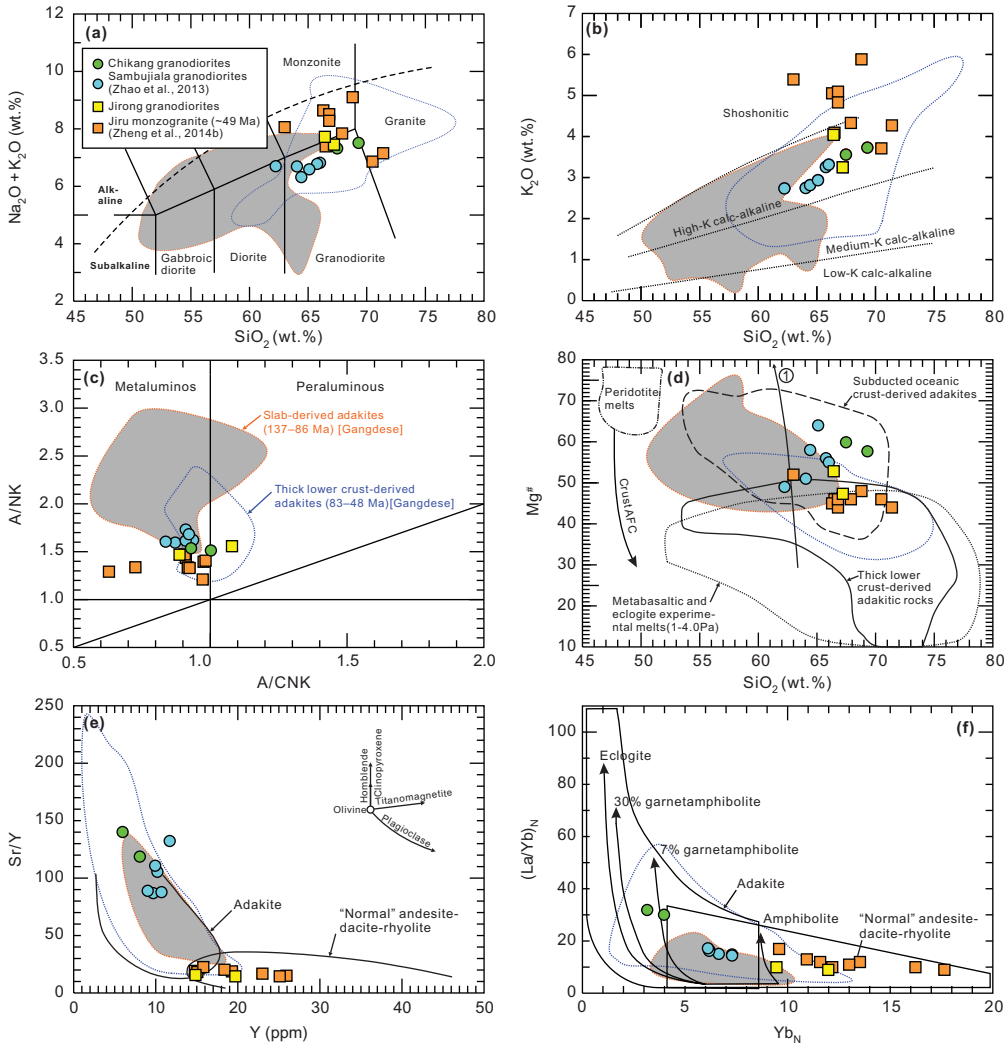

Figure 5. (a) SiO_2 *versus* $Na_2O + K_2O$ diagram (Middlemost 1994). (b) SiO_2 *versus* K_2O diagram (Peccerillo and Taylor 1976). (c) A/CNK (molar Al_2O_3/molar ($CaO + Na_2O + K_2O$)) *versus* A/NK (molar Al_2O_3/molar ($Na_2O + K_2O$)) diagram. (d) SiO_2 *versus* Mg# diagram (Wang *et al.* 2006b). (e) Y *versus* Sr/Y diagram (Defant and Drummond 1993). Crystal fractionation paths of the primary minerals are from Castillo *et al.* (1999). (f) YbN *versus* (La/Yb)N diagram. N denotes normalized to chondrite composition (Sun and McDonough 1989). The published data for the Chikang granodiorites are from Zhao *et al.* (2013) and the Jiru monzogranties are from Zheng *et al.* (2014b), respectively. The data for the slab-derived adakites in the Gangdese belt are from Zhu *et al.* (2009), Zhang *et al.* (2010a), Jiang *et al.* (2012, 2014), Ma *et al.* (2013c), and Zheng *et al.* (2014a). The data for the thick lower crust-derived adakites in the Gangdese belt are from Wen *et al.* (2008a), Guan *et al.* (2012), Ji *et al.* (2012, 2014), and Ma *et al.* (2014).

5. Discussion

5.1. Petrogenesis

5.1.1. Chikang adakitic rocks

The Chikang granodiorites have adakitic affinities (Figure 5e and f), for example high SiO_2 and Sr contents and Sr/Y and La/Yb ratios, and low Y and Yb values, and were emplaced in the Late Cretaceous (ca. 92 Ma), contemporaneously with (106–86 Ma) slab-derived adakitic rocks in the middle to eastern segment of the GBST (Zhang *et al.* 2010a; Jiang *et al.* 2012; Ma *et al.* 2013c; Chen *et al.* 2015). Adakitic rocks may be generated by a variety of mechanisms (Castillo 2012), such as melting of subducted young and hot oceanic crust (Defant and Drummond 1990), partial melting of thickened basaltic lower crust (Atherton and Petford 1993; Chung *et al.* 2003; Wang *et al.* 2005; Wen *et al.* 2008a), partial melting of delaminated lower crust (Wang *et al.* 2006a, 2006b) or subducted continental crust (Wang *et al.* 2008), crustal assimilation and low-pressure fractional crystallization from parental basaltic magmas (Castillo *et al.* 1999), high-pressure crystallization (involving garnet) of mafic magmas derived from mantle wedge peridotites (Macpherson *et al.* 2006), and magma mixing between felsic and basaltic magmas (Streck *et al.* 2007). We evaluate these alternative processes in the

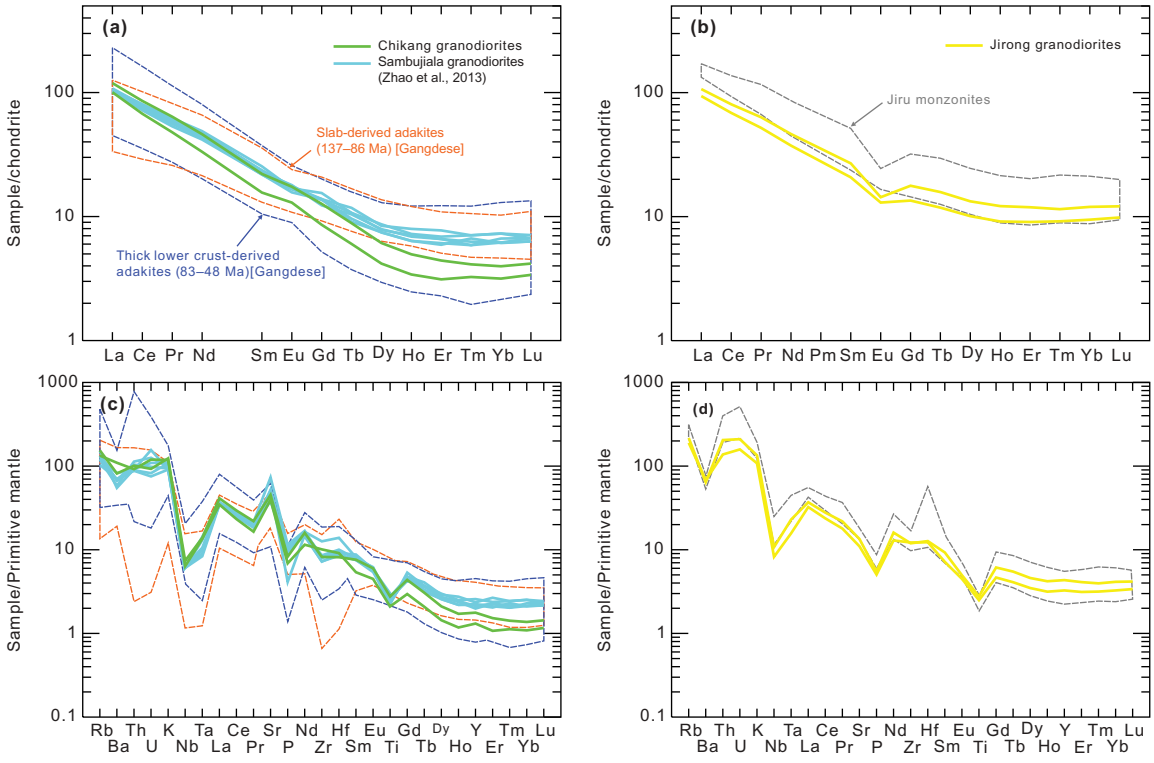

Figure 6. Chondrite-normalized rare earth element patterns and primitive mantle-normalized multi-element patterns of the Chikang–Jirong granitoids. The chondrite and primitive mantle normalization values are from Sun and McDonough (1989). Data sources are the same as for Figure 5.

following sections with specific reference to the Chikang adakitic rocks.

First, the Chikang granodiorites have MgO or Mg# (58–60) values that are distinctly higher than those of thickened lower crust-derived adakitic rocks (Figure 5d). Adakitic rocks derived by partial melting of either old thickened lower crust (Chung *et al.* 2003) or juvenile mafic lower crust beneath the GBST commonly have low MgO or Mg# values (31–50) (Hou *et al.* 2004; Wen *et al.* 2008a; Chung *et al.* 2009; Guan *et al.* 2012; Ji *et al.* 2012; Ma *et al.* 2014; Jiang *et al.* 2014), which are consistent with those of metabasalt- and eclogite-derived experimental melts (mostly $Mg^{\#} < 45$: Sen and Dunn 1994; Rapp *et al.* 1999). Moreover, the relatively high Cr (22–37 ppm) and Ni (14–23 ppm) contents of the Chikang granodiorites are distinct from those (mostly Cr <10 ppm and Ni < 7 ppm) of lower crust-derived adakitic rocks in the GBST (Wen *et al.* 2008a; Guan *et al.* 2012; Ma *et al.* 2014; Jiang *et al.* 2014). In addition, there is no geochemical or tectonic evidence that the Gangdese belt had developed thickened crust prior to 90 Ma.

Second, a scenario involving partial melting of delaminated or subducting continental lower crust is also inconsistent with the Late Cretaceous emplacement age of the Chikang granodiorites, despite their high Mg#, Cr, and Ni values. Such adakitic rocks generally occur in within-plate extensional or post-collisional settings (Wang *et al.* 2006a, 2006b, 2008), whereas the Chikang granodiorites were generated in a Late Cretaceous arc setting (Jiang *et al.* 2012; Ma *et al.* 2013a, 2013b, 2013c; Chen *et al.* 2015) at least ~20–25 million years prior to the onset of India–Asia collision. In addition, the relatively high $\varepsilon_{Hf}(t)$ (8.5–13.1) values of the Chikang granodiorites do not match those of GBST adakitc rocks ($\varepsilon_{Hf}(t) < 7$) derived by partial melting of subducted continental crust (Jiang *et al.* 2014) or delaminated lower crust in the northern Lhasa block (Wang *et al.* 2014).

Third, the Chikang granodiorites could not have been generated by high- or low-pressure crystallization from basaltic parental magmas. Adakitic rocks derived by high-pressure fractional crystallization involving garnet will generally display a distinct geochemical trend (Macpherson *et al.* 2006). Given that high-pressure crystallization involving garnet will cause a decrease in HREE and Y contents, Al_2O_3 contents will decrease and Sr/Y and Dy/Yb ratios will increase with the increasing SiO_2 contents in the evolved magmas (Macpherson *et al.* 2006). However, both Chikang and Sumbajiala granodiorites do not show such trends in their chondrite-normalized REE patterns (Figure 5a) or on Al_2O_3, Dy/Yb and Sr/Y *versus* SiO_2 diagrams (Figure 7a–c). During low-pressure

Table 3. Zircon Hf isotope data for the Chikang and Jirong pluton.

Sample	$^{176}Yb/^{177}Hf$	$^{176}Lu/^{177}Hf$	$^{176}Hf/^{177}Hf$	2σ	$(^{176}Hf/^{177}Hf)_i$	$\varepsilon_{Hf}(0)$	$\varepsilon_{Hf}(t)$	2σ	T_{DM} (Ma)	T_{DM}^{C} (Ma)	$f_{Lu/Hf}$
09TB81 01	0.023514	0.000996	0.282993	0.000017	0.282992	7.82	8.95	0.6	367	555	−0.97
09TB81 02	0.023588	0.001000	0.283008	0.000014	0.283007	8.36	9.49	0.5	345	520	−0.97
09TB81 03	0.029879	0.001210	0.282988	0.000015	0.282987	7.65	8.77	0.5	376	566	−0.96
09TB81 04	0.018619	0.000814	0.283008	0.000017	0.283007	8.35	9.48	0.6	344	520	−0.98
09TB81 05	0.025901	0.001096	0.283009	0.000014	0.283008	8.39	9.51	0.5	345	519	−0.97
09TB81 06	0.023589	0.001004	0.283004	0.000018	0.283003	8.20	9.33	0.6	352	531	−0.97
09TB81 07	0.026868	0.001155	0.282968	0.000016	0.282967	6.94	8.06	0.5	404	612	−0.97
09TB81 08	0.028845	0.001201	0.282993	0.000016	0.282992	7.83	8.95	0.6	369	555	−0.96
09TB81 09	0.032357	0.001351	0.282998	0.000015	0.282996	7.98	9.09	0.5	364	545	−0.96
09TB81 10	0.037744	0.001567	0.283003	0.000018	0.283002	8.19	9.29	0.6	358	533	−0.95
09TB81 11	0.025928	0.001094	0.283013	0.000013	0.283012	8.52	9.65	0.5	340	510	−0.97
09TB82 01	0.022796	0.000928	0.282997	0.000016	0.282996	7.96	9.09	0.6	361	546	−0.97
09TB82 02	0.022243	0.000881	0.282956	0.000022	0.282955	6.50	7.63	0.8	419	639	−0.97
09TB82 03	0.019493	0.000813	0.283009	0.000020	0.283008	8.39	9.52	0.7	342	518	−0.98
09TB82 04	0.021873	0.000881	0.283033	0.000015	0.283033	9.25	10.38	0.5	309	463	−0.97
09TB82 05	0.018853	0.000808	0.283008	0.000015	0.283007	8.36	9.49	0.5	344	520	−0.98
09TB82 06	0.018795	0.000766	0.283010	0.000018	0.283009	8.42	9.55	0.6	341	516	−0.98
09TB82 07	0.021966	0.000912	0.282991	0.000015	0.282990	7.74	8.87	0.5	369	560	−0.97
09TB82 08	0.017849	0.000705	0.282992	0.000015	0.282991	7.78	8.92	0.5	366	557	−0.98
09TB82 09	0.021797	0.000873	0.282989	0.000020	0.282988	7.68	8.81	0.7	371	563	−0.97
09TB82 10	0.016024	0.000663	0.282998	0.000020	0.282998	8.00	9.14	0.7	356	542	−0.98
09TB82 11	0.017731	0.000750	0.282985	0.000014	0.282985	7.55	8.68	0.5	375	572	−0.98
09TB82 12	0.023552	0.000927	0.283000	0.000031	0.282999	8.05	9.18	1.1	357	540	−0.97
09TB84 01	0.015755	0.000724	0.283087	0.000029	0.283086	11.15	13.12	1.0	231	316	−0.98
09TB84 02	0.016301	0.000761	0.283030	0.000017	0.283028	9.12	11.09	0.6	313	447	−0.98
09TB84 03	0.019670	0.000897	0.283038	0.000032	0.283037	9.42	11.38	1.1	302	428	−0.97
09TB84 04	0.020336	0.000924	0.283077	0.000030	0.283076	10.79	12.76	1.1	247	340	−0.97
09TB84 05	0.010313	0.000474	0.282998	0.000024	0.282997	8.00	9.99	0.9	355	518	−0.99
09TB84 06	0.022621	0.001043	0.283015	0.000019	0.283013	8.58	10.53	0.7	337	483	−0.97
09TB84 07	0.018657	0.000923	0.282956	0.000037	0.282954	6.50	8.46	1.3	419	616	−0.97
09TB84 08	0.019614	0.000912	0.283075	0.000018	0.283073	10.72	12.68	0.7	250	345	−0.97
09TB84 09	0.021117	0.000982	0.282983	0.000039	0.282981	7.45	9.41	1.4	382	555	−0.97
09TB84 10	0.017601	0.000812	0.283031	0.000019	0.283030	9.16	11.13	0.7	312	445	−0.98

Notes: $\varepsilon_{Hf}(T) = [^{176}Hf/^{177}Hf_Z / ^{176}Hf/^{177}Hf_{CHUR}(t) - 1] \times 10{,}000$;

$^{176}Hf/^{177}Hf_{CHUR}(T) = {}^{176}Hf/^{177}Hf_{CHUR}(0) - {}^{176}Lu/^{177}Hf_{CHUR} \times (e^{\lambda T} - 1)$

$T_{DM} = (1/\lambda) \times \ln[1 + (^{176}Hf/^{177}Hf_{DM} - {}^{176}Hf/^{177}Hf_Z)/(^{176}Lu/^{177}Hf_{DM} - {}^{176}Lu/^{177}Hf_Z)]$;

$T_{DM}^{C} = T_{DM} - (T_{DM} - T) \times [(f_C^{C} - f_Z)/(f_C^{C} - f_{DM})]$;

$f_{Lu/Hf} = {}^{176}Hf/^{177}Hf_Z/^{176}Lu/^{177}Hf_{CHUR} - 1$,

where f_C^{C}, f_{Zircon} and f_{DM} are the $f_{Lu/Hf}$ values of the continental crust, zircon sample and the depleted mantle; subscript Z = analysed zircon sample, CHUR = chondritic uniform reservoir; DM = depleted mantle; T = 92.8 Ma, mean age of the Milin granitoids; $\lambda = 1.867 \times 10^{-11}$ year^{-1}, decay constant of ^{176}Lu (Söderlund *et al.* 2004); $^{176}Hf/^{177}Hf_{DM} = 0.28325$; $^{176}Lu/^{177}Hf_{DM} = 0.0384$; present-day $^{176}Hf/^{177}Hf_{CHUR}(0) = 0.282772$; $^{176}Hf/^{177}Hf_{CHUR} = 0.0332$; $^{176}Hf/^{177}Hf_C^{C} = 0.015$.

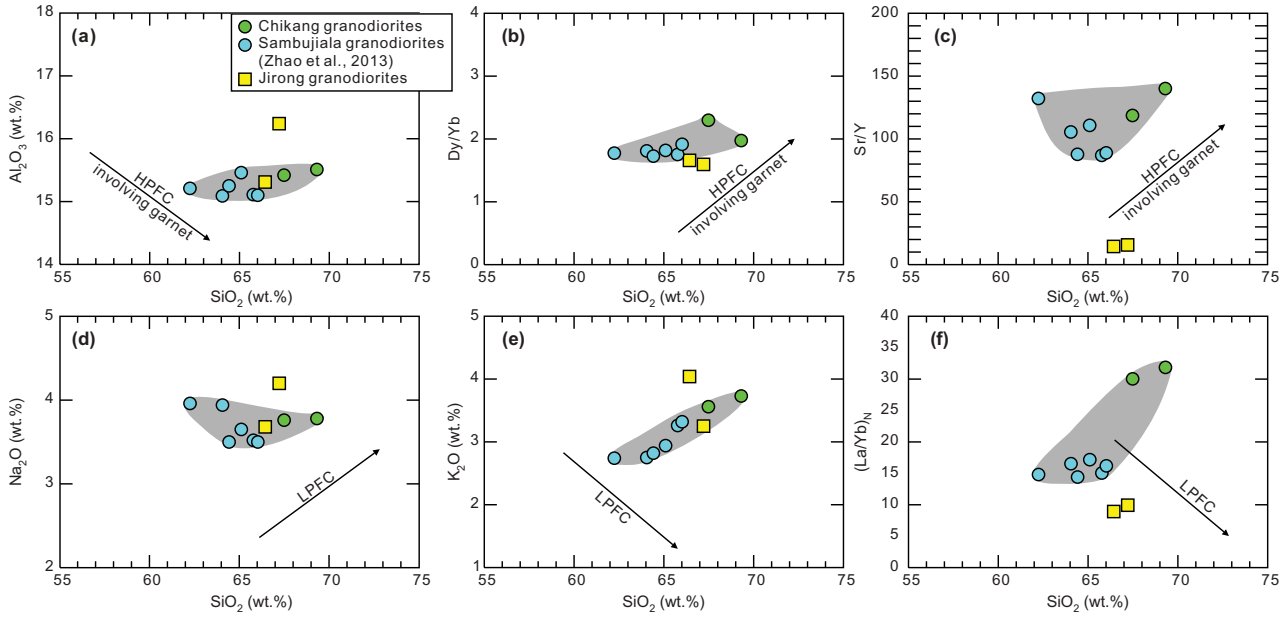

Figure 7. Plot of (a) SiO_2 *versus* Al_2O_3; (b) SiO_2 *versus* Dy/Yb; (c) SiO_2 *versus* Sr/Y; (d) Na_2O *versus* SiO_2; (e) K_2O *versus* SiO_2; and (f) SiO_2 *versus* (La/Yb)N for the Chikang–Jirong granitoids. HPFC, high-pressure fractional crystallization involving garnet (Macpherson et al. 2006); LPFC, low-pressure fractional crystallization trend (Castillo *et al.* 1999).

fractional crystallization involving olivine and pyroxene, the evolved magmas should have a marked decrease in Mg# values as well as Cr and Ni contents with the increasing SiO_2 contents (Castillo *et al.* 1999), but their Mg# values show an increasing trend (Figure 5d). Moreover, they do not exhibit the compositional trends characteristic of low-pressure fractional crystallization (Figures 7d–f) (Castillo *et al.* 1999). The flat MREE to HREE patterns do not appear to result from amphibole fractionation (Richards 2009). Amphibole fractionation ($Kd_{MREE} > Kd_{HREE}$) will decrease Dy/Yb ratios (Macpherson *et al.* 2006). In contrast, Dy/Yb ratios increase with the increasing SiO_2 contents for both Chikang and Sumbajiala adakitic granodiorites (Figure 7b). Numerous workers have pointed out that very high degrees of amphibole (>85%) and (or) garnet (>15%) fractionation are required to produce the fractionation trends observed in adakitic rocks if they are generated from fractionation processes (Bourdon *et al.* 2002; Mori *et al.* 2007). This scenario requires an enormous volume of primary basaltic parent magma to supply these minerals (Gomez-Tuena *et al.* 2007), but coeval mafic magmatism has not yet been identified in the region. In addition, the MREEs would be more depleted than HREEs, rather than the flat patterns observed in the Chikang granodiorites (Figure 5b), if abundant amphibole fractionation had occurred. Therefore, we conclude that amphibole fractionation was unlikely to have been the controlling factor in the formation of the Chikang adakitic rocks. Geochemical characteristics of the Chikang adakitic rocks also preclude significant crustal contamination in their petrogenesis. Ma *et al.* (2013b) investigated the Zhengga gabbros (ca. 94 Ma) exposed in the GBST and showed that they were generated by assimilation and fractional crystallization of olivine or clinopyroxene from hydrous melt of lithospheric mantle. However, the Chikang granodiorites have higher SiO_2 (66.8–68.3 wt.%) and $\varepsilon_{Hf}(t)$ (8.3–13.0) than those of the Zhengga gabbros (SiO_2 = 43.7–52.2 wt.%, $\varepsilon_{Hf}(t)$ = 2.9–6.5). Moreover, the Chikang granodiorites have homogeneous zircon $\varepsilon_{Hf}(t)$ ($\Delta\varepsilon_{Hf}(t)$ < 5.0) values (Figure 7, Table 3) that also preclude the model of magma mixing between mantle-derived mafic and crust-derived felsic magmas.

In view of the above, and the fact that the high MgO, Cr and Ni contents and Mg# values of the Chikang granodiorites are similar to those of Cretaceous adakitic rocks in the GBST derived from Neo-Tethyan slab (Zhu *et al.* 2009; Jiang *et al.* 2012, 2014; Ma *et al.* 2013c; Chen *et al.* 2015), we conclude that the Chikang adakitic granodiorites were also most likely generated by partial melting of subducted Neo-Tethyan Oceanic crust. Studies on tectonics, sedimentation and magmatism in the Lhasa block have demonstrated that the southern GBST, including the Chikang area, was in an arc setting during the Late Cretaceous (Kapp *et al.* 2005, 2007; Wen *et al.* 2008b; Ji *et al.* 2009b; Jiang *et al.* 2012, 2014; Ma *et al.* 2013a, 2013b, 2013c). Moreover, their high Mg# (58–60) values and Ni (14–23 ppm) and Cr (22–37 ppm) contents are similar to those (Mg# > 47, Ni = 20–40 ppm and Cr = 30–50 ppm) of subducted oceanic crust-derived adakites

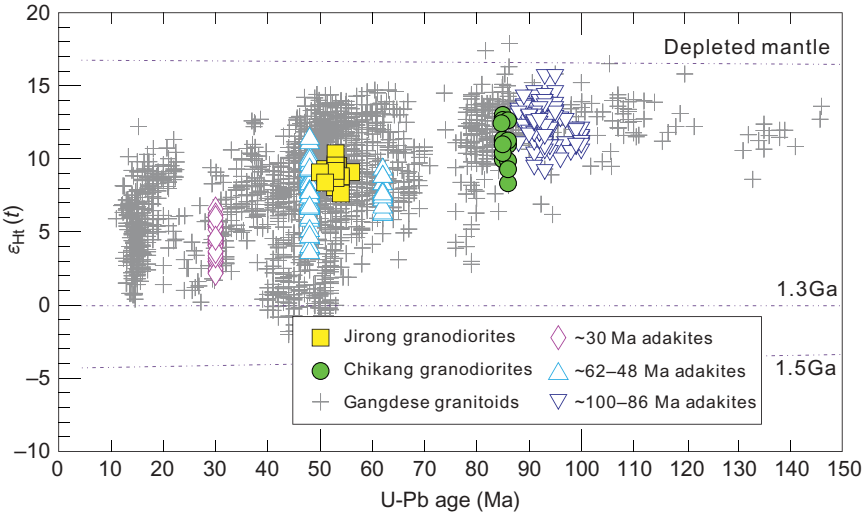

Figure 8. Plot of εHf(t) *versus* U–Pb age of zircon from the Gangdese belt. Data are from this study and literature sources (Zhang *et al.* 2007; Chung *et al.* 2009; Zhu *et al.* 2009, 2011; Ji *et al.* 2009b, 2012; Guan *et al.* 2010, 2012; Huang *et al.* 2010; Chu *et al.* 2011; Jiang *et al.* 2012, 2014; Ma *et al.* 2013c, 2014).

worldwide (Martin 1999) as well as those of the GBST. The $\varepsilon_{Hf}(t)$ values of the Chikang granodiorites are also similar to those of Cretaceous slab-derived adakitic rocks in the GBST (Figure 8) (Zhu *et al.* 2009; Jiang *et al.* 2012; Ma *et al.* 2013c; Chen *et al.* 2015).

5.1.2. *Jirong granodiorites*

The Jirong granodiorites (~53 Ma) are characterized by high SiO_2 contents (64.8–65.3 wt.%) and are high-K calc-alkaline and metaluminous to slightly peraluminous (Figure 5b and c). We propose that they were probably generated by partial melting of juvenile lower crust beneath the GBST. They have high SiO_2 and low MgO, Mg#, Cr, and Ni contents, similar to Jurassic–early Eocene calc-alkaline granitoids derived from juvenile lower crust in the GBST (Ji *et al.* 2009a, 2012). Trace element and REE patterns of the Jirong granodiorites are also similar to those of classic arc-type granitoids (Zhu *et al.* 2008), i.e. enriched in LILEs (Rb, Ba, Th, U, K) and LREEs (La, Ce) and relatively depleted in HFSEs (Nb, Ta, Ti). The depletion of Eu can be explained either by the fractional crystallization of plagioclase or the retention of residual of plagioclase in the source, while the depletion of P may reflect the crystallization of apatite (Li *et al.* 2007). The Jirong granodiorites exhibit relatively flat HREE patterns (Figure 6b), suggesting that amphibole, rather than garnet, played an important role during partial melting as a residual phase in the source (Wen *et al.* 2008a).

The Jirong granodiorites also have high $\varepsilon_{Hf}(t)$ (7.6–10.4) values with young Hf model ages (T_{DM}^{C} = 463–639 Ma), consistent with those of the Jurassic–Cretaceous calc-alkaline granitoids in the GBST (Figure 8). In particular, they have $\varepsilon_{Hf}(t)$ and T_{DM}^{C} values similar to those of Paleogene–Eocene granitoids exposed in the Zhanang–Wolong area, which mainly originated from juvenile lower crust beneath the GBST (Guan *et al.* 2012; Jiang *et al.* 2014).

5.2. *Geodynamic processes and implications for metallogenesis*

5.2.1. *Geodynamic processes*

Voluminous zircon U-Pb and whole-rock $^{40}Ar/^{39}Ar$ age data for igneous and volcanic rocks developed in the GBST suggest two significant stages of magmatic activity, i.e. ca. 100–80 Ma and ca. 65–41 Ma (Wen *et al.* 2008b; Lee *et al.* 2009; Ji *et al.* 2009b; Ma *et al.* 2013a). Various geodynamic models have been proposed for these two stages.

Wen *et al.* (2008b) proposed that the Late Cretaceous magmatic event (ca. 100–80 Ma) was linked to a geodynamic transition where subduction of the Neo-Tethyan oceanic slab changed from normal-angle (100–85 Ma) to shallow-angle subduction (85–80 Ma). Zhang *et al.* (2010a) suggested that Late Cretaceous (90–86 Ma) charnockites in the Milin–Lilong area of the GBST resulted from Neo-Tethyan mid-ocean ridge subduction. However, Ma *et al.* (2013a) suggested that contemporaneous (ca. 93 Ma) norites and hornblendites in the Milin area were generated by the interaction of upwelling asthenospheric and metasomatized lithospheric mantle due to the rollback of subducted Neo-Tethyan oceanic slab. All these processes can lead to partial melting of subducted oceanic slab. However, if the mid-ocean ridge subduction model is correct, then the lack of any age trend in the distribution of

mafic rocks and adakites (Figure 1c in Ma *et al.* 2013b) would imply a spreading ridge sub-parallel to the trench. In such a scenario, however, subduction is likely to cease because of the dominance of young buoyant oceanic crust (Thorkelson 1996), rather than lasting for over 15 Ma. Moreover, the required 70–80 km depth of slab partial melting (Sen and Dunn 1994) and continuous magmatism during the Cretaceous (Wu *et al.* 2010) are also inconsistent with the subduction angle transition model (Wen *et al.* 2008b).

We therefore prefer a model of Neo-Tethyan oceanic slab rollback during the Late Cretaceous (Figure 9a) as described in greater detail by Ma *et al.* (2013a) and Jiang *et al.* (2014). It can readily account for the contemporary Gangdese magmatic 'flare-up' event. Ma *et al.* (2013a) documented high-temperature (up to 1340°C) norites in the Milin area of the GBST, which originated from interaction between lithosphere and upwelling asthenosphere caused by rollback of the subducting Neo-Tethyan oceanic slab. Collectively, the coeval occurrence of high-temperature norites and charnockites (Ma *et al.* 2013a) with adakitic magmatism (Zhang *et al.* 2010a; Ma *et al.* 2013c) and granulite-facies metamorphism (Zhang *et al.* 2010b) in the Milin area provide strong evidence for an early Late Cretaceous regional thermal event. The upwelling of asthenosphere was possibly triggered by slab rollback though migrating backward of an asthenosphere mantle (Gvirtzman and Nur 1999). Meanwhile, asthenospheric upwelling or the triggered mantle flow probably provided the high temperature regime required for partial melting of the upper surface of subducted Neo-Tethyan oceanic slab to generate the Chikang adakitic granodiorites.

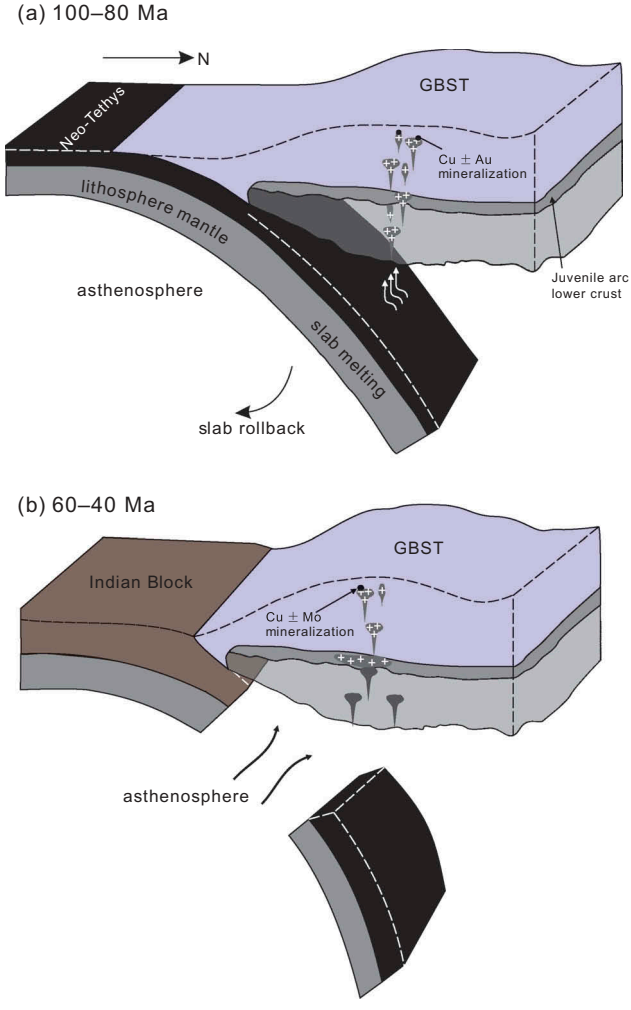

Figure 9. Model for Late Cretaceous and early Eocene geodynamic evolution and related Cu ± Au ± Mo mineralization of the Gangdese belt. (a) 100–80 Ma; rollback of subducted Neo-Tethyan oceanic lithosphere; (b) 60–40 Ma; breakoff of subducted Neo-Tethyan oceanic lithosphere. GBST, Gangdese belt of southern Tibet.

For the early Tertiary magmatic activity (ca. 65–41 Ma), we suggest that the ca. 50 Ma magmatic flare-up in the Gangdese belt was most probably related to slab break-off following Neo-Tethyan oceanic slab rollback (Figure 9b) as suggested by Lee *et al.* (2009), Chen *et al.* (2015) and Ma *et al.* (2014). The lines of evidence include the following. (1) slab break-off can readily explain the diverse geochemical characteristics of the Linzizong volcanic rocks that likely resulted from multiple magma source regions (e.g. Lee *et al.* 2012). (2) Geological mapping and geochronological data show that early Tertiary magmatic rocks crop out in a linear distribution across the southern Lhasa block. This distribution is consistent with magmatism developed after slab break-off (Chung *et al.* 2005). (3) Slab break-off can also explain why there was a decrease in the India–Asian convergence velocity during the Eocene (Lee and Lawver 1995) given that break-off would have eliminated slab pull from the existing Neo-Tethyan subdution zone and consequently prevented subduction of the Indian continental lithosphere beneath southern Tibet. (4) The occurrence of ultrahigh-pressure rock is consistent with Eocene slab break-off, as proposed by previous workers based on Himalayan metamorphic records (Kohn and Parkinson 2002; Guillot *et al.* 2003). Leech *et al.* (2005) suggested that the ca. 53 Ma ultrahigh-pressure rocks in the northwestern Himalaya result from early, steep continental subduction and proposed that oceanic slab break-off broadly coincided with exhumation of the ultrahigh-pressure rocks in this region. (5) Eocene slab break-off also could explain early Tertiary topographic uplift in southern Tibet (Lee *et al.* 2009; Smit *et al.* 2014).

5.2.2. *Implications for metallogenesis*

Zircon U–Pb dating of the Chikang adakitic graodiorites indicates that they were generated in the Late Cretaceous (ca. 92 Ma) and therefore were contemporaneous with the Late Cretaceous (ca. 100–80 Ma) magmatic 'flare-up' in the central and eastern segments of the GBST (Ma *et al.*

Table 4. Summary of the 106–86 Ma slab-derived adakites in the Gangdese belt of Lhasa block.

Location	Rock type	Dating method	Age (Ma)	Geochemcial affinity	References
Kelu	Quartz monzonite Diorite	Zircon LA ICPMS U–Pb	93–90	Mg# = 57 – 61 $\varepsilon_{Nd}(t)$ = +3.0 – +4.4 $\varepsilon_{Hf}(t)$ = +9.3 – +15.8	Jiang *et al.* (2012)
Sambujiala	Granodiorite	Zircon LA ICPMS U–Pb	92.1 ± 0.6	Mg# = 49 – 64	Zhao *et al.* (2013)
Lilong–Milin	Granodiorite Diorite	Zircon LA ICPMS U–Pb	100–89	Mg# = 46 – 56 $\varepsilon_{Nd}(t)$ = +2.4 – +4.0 $\varepsilon_{Hf}(t)$ = +10.1 – +15.8	Ma *et al.* (2013c)
Lilong–Milin	Charnockite	Zircon LA ICPMS U–Pb	90–86	Mg# = 50 – 54	Zhang *et al.* (2010a)
Nuri	Quartz diorite	Zircon LA ICPMS U–Pb	95.9 ± 0.9	Mg# = 48 – 64 $\varepsilon_{Nd}(t)$ = +2.7 – +2.8 $\delta^{18}O$ = +8.9 – +9.2	Zheng *et al.* (2014a)
Chikang	Granodiorite	Zircon LA ICPMS U–Pb	85.6 ± 1.5	Mg# = 58 – 60 $\varepsilon_{Hf}(t)$ = +8.5 – +13.1	This paper
Nuri	Felsophyre Quartz diorites	Zircon LA ICPMS U–Pb	106–93	Mg# = 48 – 60 $\varepsilon_{Nd}(t)$ = +3.1 – +3.5 $\varepsilon_{Hf}(t)$ = +3.7 – +15.5	Chen *et al.* (2015)

2013a). The existing geochronological and geochemical data for Late Cretaceous igneous rocks exposed in the GBST show that voluminous ca. 106–86 Ma slab-derived adakitic rocks developed along the central and eastern sectors of the GBST (Table 4), including quartz diorites, felsophyres, and quartz diorite porphyrites from Nuri (ca. 106–93 Ma; Chen *et al.* 2015), granodiorites and diorites from Lilong–Milin (ca. 100–86 Ma; Zhang *et al.* 2010a; Ma *et al.* 2013c; Zheng *et al.* 2014a), quartz monzonites and diorites from Kelu (ca. 93–90 Ma; Jiang *et al.* 2012), and granodiorites from Sambujiala (ca. 92 Ma; Liang *et al.* 2010; Zhao *et al.* 2013). Moreover, abundant ca. 100–80 Ma zircon xenocrysts in the Sailipu Miocene ultra-K volcanic rocks (Liu *et al.* 2014) also indicated the presence of magmatic activity at ca. 100–80 Ma in the western GBST. Accordingly, ca. 90 Ma slab-derived adakitic magmatism likely developed along the entire southern margin of the GBST. Jiang *et al.* (2012) first reported the occurrence of the Kelu skarn Cu–Au deposits associated with the Late Cretaceous (~90 Ma) Neo-Tethyan slab-derived adakitic rocks. Subsequently, the Sumbajiala skarn Cu–Au deposit was also attributed to the ca. 90 Ma slab-derived adakitic rocks (Zhao *et al.* 2013). These recent discoveries indicate that the ca. 106–86 Ma slab-derived adakitic rocks in the GBST have significant potential for Cu–Au mineralization.

Based on the detailed comparisons of post-collisional fertile and barren porphyry systems in the GBST, Hou *et al.* (2013) proposed that the fertile magmas were most likely derived by partial melting of a thickened juvenile mafic lower crust, formed by the underplating of earlier asthenospheric melts at the base of the crust. The Sr–Nd–Hf isotopic data for the fertile magmatic rocks show a greater than 70% mantle contribution to the source of the ore-related magmatic rocks (Hou *et al.* 2013). These results emphasize the significant contribution of juvenile mantle components to the Cu mineralization. Richards (2009) proposed that the remelting and remobilization of mantle components in juvenile crust, including sulphide-bearing phases, most likely provided Cu-Au and S for the collisional zone porphyry systems. Numerous studies have shown that, as a result of the Neo-Tethyan slab rollback (Ma *et al.* 2013a, 2013b), Late Cretaceous (ca. 100–80 Ma) mafic magmatism from the asthenospheric mantle was emplaced into the base of the Gangdese arc and strongly reworked the lower crust. As previously noted, numerous zircon U–Pb ages in the Gangdese belt show that there was a second magmatic peak at 50 Ma, which was generated by partial melting of underplated juvenile lower crust as a result of slab break-off (Wen *et al.* 2008b; Ji *et al.* 2009b, 2012). As a result, the Gangdese arc lower crust underwent additional intense reworking (Ji *et al.* 2009a; Lee *et al.* 2012: Ma *et al.* 2014). Thus, voluminous asthenospheric material was transferred to the lower crust though the processes of slab rollback and break-off. The Jiru porphyry Cu ± Mo deposits (Zheng *et al.* 2014b) and Sharang Mo deposits (Zhao *et al.* 2014) demonstrate that this Eocene period of magmatism also has important potential for Cu ± Mo mineralization.

Since the late 1990s, most Cu ± Au ± Mo deposits discovered in the GBST were attributed to an extensional setting following India–Asia collision (Hou *et al.* 2009). The increasingly recognized Late Cretaceous and Eocene Cu ± Au ± Mo mineralization events, however, demonstrate that the Gangdese porphyry copper belt also contains subduction- and collision-related porphyry/

skarn-type Cu ± Au ± Mo deposits. Thus, Late Cretaceous and Eocene intrusive rocks should be targeted as important potential hosts for Cu ± Au ± Mo mineralization during mineral exploration.

6. Conclusions

New zircon U–Pb ages indicate that the Chikang and Jirong granodiorites were emplaced at ca. 92 Ma and ca. 53 Ma, respectively. The Chikang granodiorites show geochemical features typical of slab-derived adakites and were most probably produced by partial melting of subducted oceanic crust, followed by subsequent adakitic melt–mantle interactions. The Jirong granodiorites were likely generated by partial melting of juvenile crustal materials. The two episodes of magmatism were generated in response to the rollback and subsequent break-off of Neo-Tethyan oceanic lithosphere, respectively. The Late Cretaceous–Eocene magmatic rocks in the GBST have important potential for Cu ± Au ± Mo mineralization.

Acknowledgements

We appreciate the assistance of Ying Liu, Guangqian Hu, and Xianglin Tu for geochemical analyses. Editor Robert Stern and two anonymous reviewers are kindly thanked for their thorough reviews and constructive criticisms.

Disclosure statement

No potential conflict of interest was reported by the author(s).

Funding

This study was jointly supported by the Strategic Priority Research Programme (B) of the Chinese Academy of Sciences [grant number XDB03010600]; the National Natural Science Foundation of China [grant number 41025006], [grant number 41421062], [grant number 41202040]; the Guangzhou Institute of Geochemistry, Chinese Academy of Sciences [GIGCAS 135 project Y234021001]. This is contribution No. IS–2028 from GIGCAS.

References

Andersen, T., 2002, Correction of common lead in U–Pb analyses that do not report ^{204}Pb: Chemical Geology, v. 192, p. 59–79. doi:10.1016/S0009-2541(02)00195-X.

Atherton, M.P., and Petford, N., 1993, Generation of sodium-rich magmas from newly underplated basaltic crust: Nature, v. 362, p. 144–146. doi:10.1038/362144a0.

Bourdon, E., Eissen, J.P., Monzier, M., Robin, C., Martin, H., Cotton, J., and Hall, M.L., 2002, Adakite-like lavas from Antisana Volcano (Ecuador): Evidence from slab melt metasomatism beneath the Andean northern volcanic zone: Journal of Petrology, v. 43, p. 199–217. doi:10.1093/petrology/43.2.199.

Castillo, P.R., 2012, Adakite petrogenesis: Lithos, v. 134–135, p. 304–316. doi:10.1016/j.lithos.2011.09.013.

Castillo, P.R., Janney, P.E., and Solidum, R.U., 1999, Petrology and geochemistry of Camiguin Island, southern Philippines: Insights to the source of adakites and other lavas in a complex arc setting: Contributions to Mineralogy and Petrology, v. 134, p. 33–51. doi:10.1007/s004100050467.

Chen, L., Qin, K.Z., Li, G.M., Li, J.X., Xiao, B., Zhao, J.X., and Fan, X., 2015, Zircon U–Pb ages, geochemistry and Sr–Nd–Pb–Hf isotopes of Nuri 1 intrusive rocks in Gangdese area, southern Tibet: Constraints on timing, petrogenesis and tectonic transformation: Lithos, v. 212–215, p. 379–396. doi:10.1016/j.lithos.2014.11.014.

Chen, L., Qin, K.Z., Li, J.X., Xiao, B., Li, G.M., Zhao, J.X., and Fan, X., 2012, Fluid inclusions and hydrogen, oxygen, sulfur isotopes of Nuri Cu–W–Mo deposit in the Southern Gangdese, Tibet: Resource Geology, v. 62, p. 42–62. doi:10.1111/j.1751-3928.2011.00179.x.

Chu, M.-F., Chung, S.-L., O'Reilly, S.Y., Pearson, N.J., Wu, F.-Y., Li, X.-H., Liu, D.Y., Ji, J.Q., Chu, C.-H., and Lee, H.-Y., 2011, India's hidden inputs to Tibetan orogeny revealed by Hf isotopes of Transhimalayan zircons and host rocks: Earth and Planetary Science Letters, v. 307, p. 479–486. doi:10.1016/j.epsl.2011.05.020.

Chung, S.-L., Chu, M.-F., Ji, J.Q., O'Reilly, S.Y., Pearson, N.J., Liu, D.Y., Lee, T.-Y., and Lo, C.-H., 2009, The nature and timing of crustal thickening in Southern Tibet: Geochemical and zircon Hf isotopic constraints from postcollisional adakites: Tectonophysics, v. 477, p. 36–48. doi:10.1016/j.tecto.2009.08.008.

Chung, S.-L., Chu, M.-F., Zhang, Y.Q., Xie, Y.W., Lo, C.-H., Lee, T.-Y., Lan, C.-Y., Li, X.H., Zhang, Q., and Wang, Y.Z., 2005, Tibetan tectonic evolution inferred from spatial and temporal variations in post-collisional magmatism: Earth-Science Reviews, v. 68, p. 173–196. doi:10.1016/j.earscirev.2004.05.001.

Chung, S.-L., Liu, D.Y., Ji, J.Q., Chu, M.-F., Lee, H.-Y., Wen, D.-J., Lo, C.-H., Lee, T.-Y., Qian, Q., and Zhang, Q., 2003, Adakites from continental collision zones: Melting of thickened lower crust beneath southern Tibet: Geology, v. 31, p. 1021–1024. doi:10.1130/G19796.1.

Cooke, D., Hollings, P., and Walshe, J., 2005, Giant porphyry deposits: Characteristics, distribution, and tectonic controls: Economic Geology, v. 100, p. 801–818. doi:10.2113/gsecongeo.100.5.801.

Corfu, F., Hanchar, J.M., Hoskin, P.W., and Kinny, P., 2003, Atlas of zircon textures: Reviews in Mineralogy and Geochemistry, v. 53, p. 469–500. doi:10.2113/0530469.

DeCelles, P.G., Kapp, P., Ding, L., and Gehrels, G.E., 2007, Late Cretaceous to middle Tertiary basin evolution in the central Tibetan Plateau: Changing environments in response to tectonic partitioning, aridification, and regional elevation gain: Geological Society of America Bulletin, v. 119, p. 654–680. doi:10.1130/B26074.1.

Defant, M.J., and Drummond, M.S., 1990, Derivation of some modern arc magmas by melting of young subducted lithosphere: Nature, v. 347, p. 662–665. doi:10.1038/347662a0.

Defant, M.J., and Drummond, M.S., 1993, Mount St. Helens: Potential example of the partial melting of the subducted lithosphere in a volcanic arc: Geology, v. 21, p. 547–550. doi:10.1130/0091-7613(1993)021<0547:MSHPEO>2.3.CO;2.

Gomez-Tuena, A., Langmuir, C.H., Goldstein, S.L., Straub, S.M., and Ortega-Gutierrez, F., 2007, Geochemical evidence for slab melting in the Trans-Mexican volcanic belt: Journal of Petrology, v. 48, p. 537–562. doi:10.1093/petrology/egl071.

Guan, Q., Zhu, D.-C., Zhao, Z.-D., Dong, G.-C., Zhang, L.-L., Li, X.-W., Liu, M., Mo, X.-X., Liu, Y.-S., and Yuan, H.-L., 2012, Crustal thickening prior to 38 Ma in southern Tibet: Evidence from lower crust-derived adakitic magmatism in the Gangdese Batholith: Gondwana Research, v. 21, p. 88–99. doi:10.1016/j.gr.2011.07.004.

Guan, Q., Zhu, D.C., Zhao, Z.D., Zhang, L.L., Liu, M., Li, X.W., Yu, F., and Mo, X.X., 2010, Late Cretaceous adakites in the eastern segment of the Gangdese Belt, southern Tibet: Products of Neo-Tethyan ridge subduction?: Acta Petrologica Sinica, v. 26, p. 2165–2179. [In Chinese with English Abstract.]

Guillot, S., Garzanti, E., Baratoux, D., Marquer, D., Mahéo, G., and De Sigoyer, J., 2003, Reconstructing the total shortening history of the NW Himalaya: Geochemistry, Geophysics, Geosystems, v. 4. doi:10.1029/2002GC000484.

Gvirtzman, Z., and Nur, A., 1999, The formation of Mount Etna as the consequence of slab rollback: Nature, v. 401, p. 782–785. doi:10.1038/44555.

Hoskin, P.W.O., and Schaltegger, U., 2003, The composition of zircon and igneous and metamorphic petrogenesis: Reviews in Mineralogy and Geochemistry, v. 53, p. 27–62. doi:10.2113/0530027.

Hou, Z.-Q., Gao, Y.-F., Qu, X.-M., Rui, Z.-Y., and Mo, X.-X., 2004, Origin of adakitic intrusives generated during mid-Miocene east-west extension in southern Tibet: Earth and Planetary Science Letters, v. 220, p. 139–155. doi:10.1016/S0012-821X(04)00007-X.

Hou, Z.Q., Yang, Z.M., Qu, X.M., Meng, X.J., Li, Z.Q., Beaudoin, G., Rui, Z.Y., Gao, Y.F., and Zaw, K., 2009, The Miocene Gangdese porphyry copper belt generated during post-collisional extension in the Tibetan orogen: Ore Geology Reviews, v. 36, p. 25–51. doi:10.1016/j.oregeorev.2008.09.006.

Hou, Z.Q., Zheng, Y.C., Yang, Z.M., Rui, Z.Y., Zhao, Z.D., Jiang, S.H., Qu, X.M., and Sun, Q.Z., 2013, Contribution of mantle components within juvenile lower-crust to collisional zone porphyry Cu systems in Tibet: Mineralium Deposita, v. 48, p. 173–192. doi:10.1007/s00126-012-0415-6.

Huang, Y., Zhao, Z.D., Zhang, F.Q., Zhu, D.C., Dong, G.C., and Mo, X.X., 2010, Geochemistry and implication of the Gangdese batholiths from Renbu and Lhasa areas in southern Gangdese, Tibet: Acta Petrologica Sinica, v. 26, p. 3131–3142. [In Chinese with English Abstract.]

Jackson, S.E., Pearson, N.J., Griffin, W.L., and Belousova, E.A., 2004, The application of laser ablation-inductively coupled plasma-mass spectrometry to in situ U–Pb zircon geochronology: Chemical Geology, v. 211, p. 47–69. doi:10.1016/j.chemgeo.2004.06.017.

Ji, W.-Q., Wu, F.-Y., Chung, S.-L., Li, J.-X., and Liu, C.-Z., 2009b, Zircon U–Pb geochronology and Hf isotopic constraints on petrogenesis of the Gangdese batholith, southern Tibet: Chemical Geology, v. 262, p. 229–245. doi:10.1016/j.chemgeo.2009.01.020.

Ji, W.Q., Wu, F.Y., Liu, C.Z., and Chung, S.L., 2009a, Geochronology and petrogenesis of granitic rocks in Gangdese batholith, southern Tibet Science in China Series D: Earth Sciences, v. 52, p. 1240–1261. doi:10.1007/s11430-009-0131-y.

Ji, W.-Q., Wu, F.-Y., Liu, C.-Z., and Chung, S.-L., 2012, Early Eocene crustal thickening in southern Tibet: New age and geochemical constraints from the Gangdese batholith: Journal of Asian Earth Sciences, v. 53, p. 82–95. doi:10.1016/j.jseaes.2011.08.020.

Jiang, Z.-Q., Wang, Q., Li, Z.-X., Wyman, D.A., Tang, G.-J., Jia, X.-H., and Yang, Y.-H., 2012, Late Cretaceous (ca. 90 Ma) adakitic intrusive rocks in the Kelu area, Gangdese belt (southern Tibet): Slab melting and implications for Cu–Au mineralization: Journal of Asian Earth Sciences, v. 53, p. 67–81. doi:10.1016/j.jseaes.2012.02.010.

Jiang, Z.-Q., Wang, Q., Wyman, D.A., Li, Z.-X., Yang, J.-H., Shi, X.-B., Ma, L., Tang, G.-J., Gou, G.-N., Jia, X.-H., and Guo, H.-F., 2014, Transition from oceanic to continental lithosphere subduction in southern Tibet: Evidence from the Late Cretaceous–early Oligocene (~91–30 Ma) intrusive rocks in the Chanang–Zedong area, southern Gangdese: Lithos, v. 196-197, p. 213–231. doi:10.1016/j.lithos.2014.03.001.

Kang, Z.Q., Xu, J.F., Chen, J.L., Wang, B.D., and Dong, Y.H., 2010, The geochronology of Sangri Group volcanic rocks in Tibet: Constraints from later Mamen intrusions: Geochimica, v. 39, p. 520–530. [In Chinese with English Abstract.]

Kang, Z.-Q., Xu, J.-F., Wilde, S.A., Feng, Z.-H., Chen, J.-L., Wang, B.-D., Fu, W.-C., and Pan, H.-B., 2014, Geochronology and geochemistry of the Sangri Group Volcanic Rocks, Southern Lhasa Terrane: Implications for the early subduction history of the Neo-Tethys and Gangdese Magmatic Arc: Lithos, v. 200–201, p. 157–168. doi:10.1016/j.lithos.2014.04.019.

Kapp, P., DeCelles, P.G., Gehrels, G.E., Heizler, M., and Ding, L., 2007, Geological records of the Lhasa–Qiangtang and Indo–Asian collisions in the Nima area of central Tibet: Geological Society of America Bulletin, v. 119, p. 917–933. doi:10.1130/B26033.1.

Kapp, P., Yin, A., Harrison, T.M., and Ding, L., 2005, Cretaceous–Tertiary shortening, basin development, and volcanism in central Tibet: Geological Society of America Bulletin, v. 117, p. 865–878. doi:10.1130/B25595.1.

Kohn, M.J., and Parkinson, C.D., 2002, Petrologic case for Eocene slab breakoff during the Indo–Asian collision: Geology, v. 30, p. 591–594. doi:10.1130/0091-7613(2002)030<0591:PCFESB>2.0.CO;2.

Lang, X.H., Tang, J.X., Li, Z.J., Huang, Y., Ding, F., Yang, H.H., Xie, F.W., Zhang, L., Wang, Q., and Zhou, Y., 2014, U–Pb and Re–Os geochronological evidence for the Jurassic porphyry metallogenic event of the Xiongcun district in the Gangdese porphyry copper belt, southern Tibet, PRC: Journal of Asian Earth Sciences, v. 79 (Part B), p. 608–622, doi:10.1016/j.jseaes.2013.08.009.

Lee, H.-Y., Chung, S.-L., Ji, J.Q., Qian, Q., Gallet, S., Lo, C.-H., Lee, T.-Y., and Zhang, Q., 2012, Geochemical and Sr-Nd isotopic constraints on the genesis of the Cenozoic Linzizong volcanic successions, southern Tibet: Journal of Asian Earth Sciences, v. 53, p. 96–114. doi:10.1016/j.jseaes.2011.08.019.

Lee, H.-Y., Chung, S.-L., Lo, C.-H., Ji, J.Q., Lee, T.-Y., Qian, Q., and Zhang, Q., 2009, Eocene Neotethyan slab breakoff in southern Tibet inferred from the Linzizong volcanic record: Tectonophysics, v. 477, p. 20–35. doi:10.1016/j.tecto.2009.02.031.

Lee, T.-Y., and Lawver, L.A., 1995, Cenozoic plate reconstruction of Southeast Asia: Tectonophysics, v. 251, p. 85–138. doi:10.1016/0040-1951(95)00023-2.

Leech, M.L., Singh, S., Jain, A., Klemperer, S.L., and Manickavasagam, R., 2005, The onset of India–Asia continental collision: Early, steep subduction required by the timing of UHP metamorphism in the western Himalaya: Earth and Planetary Science Letters, v. 234, p. 83–97. doi:10.1016/j.epsl.2005.02.038.

Leng, C.-B., Zhang, X.-C., Zhong, H., Hu, R.-Z., Zhou, W.-D., and Li, C., 2013, Re–Os molybdenite ages and zircon Hf isotopes of the Gangjiang porphyry Cu–Mo deposit in the

Tibetan Orogen: Mineralium Deposita, v. 48, p. 585–602. doi:10.1007/s00126-012-0448-x.

Li, X.-H., Li, Z.-X., Li, W.-X., Liu, Y., Yuan, C., Wei, G.J., and Qi, C.S., 2007, U–Pb zircon, geochemical and Sr–Nd–Hf isotopic constraints on age and origin of Jurassic I- and A-type granites from central Guangdong, SE China: A major igneous event in response to foundering of a subducted flat-slab?: Lithos, v. 96, p. 186–204. doi:10.1016/j.lithos.2006.09.018.

Li, X.H., Qi, C.S., Liu, Y., Liang, X.R., Tu, X.L., Xie, L.W., and Yang, Y.H., 2005, Petrogenesis of the Neoproterozoic bimodal volcanic rocks along the western margin of the Yangtze Block: New constraints from Hf isotopes and Fe/Mn ratios: Chinese Science Bulletin, v. 50, p. 2481–2486. doi:10.1360/982005-287.

Li, X.-H., Zhou, H.W., Chung, S.-L., Lo, C.-H., Wei, G.J., Liu, Y., and Lee, C.-Y., 2002, Geochemical and Sr-Nd isotopic characteristics of late Paleogene ultrapotassic magmatism in southeastern Tibet: International Geology Review, v. 44, p. 559–574. doi:10.2747/0020-6814.44.6.559.

Liang, H.Y., Wei, Q.R., Xu, J.F., Hu, G.Q., and Charllote, A., 2010, Study on zircon LA-ICP-MS U–Pb age of skarn Cu mineralization related intrusion in the southern margin of the Gangdese ore belt, Tibet and its geological implication: Acta Petrologica Sinica, v. 26, p. 1692–1698. [In Chinese with English Abstract.]

Liu, D., Zhao, Z.D., Zhu, D.-C., Niu, Y.L., and Harrison, T.M., 2014, Zircon xenocrysts in Tibetan ultrapotassic magmas: Imaging the deep crust through time: Geology, v. 42, p. 43–46. doi:10.1130/G34902.1.

Ludwig, K.R., 2003, User's Manual for Isoplot 3.0: A Geochronological Toolkit for Microsoft Excel: Berkeley Geochronology Center, Special publication, v. 4, p. 1–71.

Ma, L., Wang, B.-D., Jiang, Z.-Q., Wang, Q., Li, Z.-X., Wyman, D.A., Zhao, S.-R., Yang, J.-H., Gou, G.-N., and Guo, H.-F., 2014, Petrogenesis of the Early Eocene adakitic rocks in the Napuri area, southern Lhasa: Partial melting of thickened lower crust during slab break-off and implications for crustal thickening in southern Tibet: Lithos, v. 196–197, p. 321–338. doi:10.1016/j.lithos.2014.02.011.

Ma, L., Wang, Q., Li, Z.X., Wyman, D.A., Jiang, Z.Q., Yang, J.H., Gou, G.N., and Guo, H.F., 2013a, Early Late Cretaceous (ca. 93 Ma) norites and hornblendites in the Milin area, eastern Gangdese: Lithosphere–asthenosphere interaction during slab roll-back and an insight into early Late Cretaceous (ca. 100–80 Ma) magmatic "flare-up" in southern Lhasa (Tibet): Lithos, v. 172–173, p. 17–30. doi:10.1016/j.lithos.2013.03.007.

Ma, L., Wang, Q., Wyman, D.A., Jiang, Z.-Q., Yang, J.-H., Li, Q.-L., Gou, G.-N., and Guo, H.-F., 2013b, Late Cretaceous crustal growth in the Gangdese area, southern Tibet: Petrological and Sr–Nd–Hf–O isotopic evidence from Zhengga diorite–gabbro: Chemical Geology, v. 349–350, p. 54–70. doi:10.1016/j.chemgeo.2013.04.005.

Ma, L., Wang, Q., Wyman, D.A., Li, Z.-X., Jiang, Z.-Q., Yang, J.-H., Gou, G.-N., and Guo, H.-F., 2013c, Late Cretaceous (100–89Ma) magnesian charnockites with adakitic affinities in the Milin area, eastern Gangdese: Partial melting of subducted oceanic crust and implications for crustal growth in southern Tibet: Lithos, v. 175–176, p. 315–332. doi:10.1016/j.lithos.2013.04.006.

Macpherson, C.G., Dreher, S.T., and Thirlwall, M.F., 2006, Adakites without slab melting: High pressure differentiation of island arc magma, Mindanao, the Philippines: Earth and Planetary Science Letters, v. 243, p. 581–593. doi:10.1016/j.epsl.2005.12.034.

Martin, H., 1999, Adakitic magmas: Modern analogues of Archaean granitoids: Lithos, v. 46, p. 411–429. doi:10.1016/S0024-4937(98)00076-0.

Middlemost, E.A.K., 1994, Naming materials in the magma/igneous rock system: Earth Science Reviews, v. 37, p. 215–224. doi:10.1016/0012-8252(94)90029-9.

Mo, X.X., Hou, Z.Q., Niu, Y.L., Dong, G.C., Qu, X.M., Zhao, Z.D., and Yang, Z.M., 2007, Mantle contributions to crustal thickening during continental collision: Evidence from Cenozoic igneous rocks in southern Tibet: Lithos, v. 96, p. 225–242. doi:10.1016/j.lithos.2006.10.005.

Mo, X.X., Niu, Y.L., Dong, G.C., Zhao, Z.D., Hou, Z.Q., Su, Z., and Ke, S., 2008, Contribution of syncollisional felsic magmatism to continental crust growth: A case study of the Paleogene Linzizong volcanic Succession in southern Tibet: Chemical Geology, v. 250, p. 49–67. doi:10.1016/j.chemgeo.2008.02.003.

Mori, L., Gomez-Tuena, A., Cai, Y., and Goldstein, S.L., 2007, Effects of prolonged flat subduction on the Miocene magmatic record of the central Trans-Mexican Volcanic Belt: Chemical Geology, v. 244, p. 452–473. doi:10.1016/j.chemgeo.2007.07.002.

Najman, Y., Appel, E., Boudagher-Fadel, M., Bown, P., Carter, A., Garzanti, E., Godin, L., Han, J.T., Liebke, U., Oliver, G., Parrish, R., and Vezzoli, G., 2010, Timing of India–Asia collision: Geological, biostratigraphic, and palaeomagnetic constraints: Journal of Geophysical Research-Solid Earth, v. 115, p. B12416. 10.1029/2010JB007673.

Peccerillo, A., and Taylor, S., 1976, Geochemistry of Eocene calc-alkaline volcanic rocks from the Kastamonu area, northern Turkey: Contributions to Mineralogy and Petrology, v. 58, p. 63–81. doi:10.1007/BF00384745.

Qu, X.M., Hou, Z.Q., and Li, Y.G., 2004, Melt components derived from a subducted slab in late orogenic ore-bearing porphyries in the Gangdese copper belt, southern Tibetan plateau: Lithos, v. 74, p. 131–148. doi:10.1016/j.lithos.2004.01.003.

Rapp, R.P., Shimizu, N., Norman, M.D., and Applegate, G.S., 1999, Reaction between slab-derived melts and peridotite in the mantle wedge: Experimental constraints at 3.8 GPa: Chemical Geology, v. 160, p. 335–356. doi:10.1016/S0009-2541(99)00106-0.

Richards, J.P., 2009, Postsubduction porphyry Cu-Au and epithermal Au deposits: Products of remelting of subduction-modified lithosphere: Geology, v. 37, p. 247–250. doi:10.1130/G25451A.1.

Sen, C., and Dunn, T., 1994, Dehydration melting of a basaltic composition amphibolite at 1.5 and 2.0 GPa: Implications for the origin of adakites: Contributions to Mineralogy and Petrology, v. 117, p. 394–409. doi:10.1007/BF00307273.

Sillitoe, R.H., 2010, Porphyry copper systems: Economic Geology, v. 105, p. 3–41. doi:10.2113/gsecongeo.105.1.3.

Smit, M.A., Hacker, B.R., and Lee, J., 2014, Tibetan garnet records early Eocene initiation of thickening in the Himalaya: Geology, v. 42, p. 591–594. doi:10.1130/G35524.1.

Söderlund, U., Patchett, P.J., Vervoort, J.D., and Isachsen, C.E., 2004, The ^{176}Lu decay constant determined by Lu–Hf and U–Pb isotope systematics of Precambrian mafic intrusions: Earth and Planetary Science Letters, v. 219, p. 311–324. doi:10.1016/S0012-821X(04)00012-3.

Streck, M.J., Leeman, W.P., and Chesley, J., 2007, High-magnesian andesite from Mount Shasta: A product of

magma mixing and contamination, not a primitive mantle melt: Geology, v. 35, p. 351–354. doi:10.1130/G23286A.1.

Streckeisen, A.L., 1976, Classification of the common igneous rocks by means of their chemical composition: A provisional attempt: Neues Jahrbuch fur Mineralogie, Monatshefte, v. H. 1, p. 1–15.

Sun, S.-S., and McDonough, W.F., 1989, Chemical and isotopic systematics of oceanic basalts: Implications for mantle composition and processes: Geological Society, London, Special Publications, v. 42, p. 313–345. doi:10.1144/GSL.SP.1989.042.01.19.

Tafti, R., Mortensen, J.K., Lang, J.R., Rebagliati, M., and Oliver, J.L., 2009, Jurassic U–Pb and Re–Os ages for the newly discovered Xietongmen Cu–Au porphyry district, Tibet, PRC: Implications for metallogenic epochs in the Southern Gangdese Belt: Economic Geology, v. 104, p. 127–136. doi:10.2113/gsecongeo.104.1.127.

Thorkelson, D.J., 1996, Subduction of diverging plates and the principles of slab window formation: Tectonophysics, v. 255, p. 47–63. doi:10.1016/0040-1951(95)00106-9.

Wang, Q., McDermott, F., Xu, J.-F., Bellon, H., and Zhu, Y.-T., 2005, Cenozoic K-rich adakitic volcanic rocks in the Hohxil area, northern Tibet: Lower-crustal melting in an intracontinental setting: Geology, v. 33, p. 465–468. doi:10.1130/G21522.1.

Wang, Q., Wyman, D.A., Xu, J.F., Dong, Y.H., Vasconcelos, P. M., Pearson, N., Wan, Y.S., Dong, H., Li, C.F., Yu, Y.S., Zhu, T.X., Feng, X.T., Zhang, Q.Y., Zi, F., and Chu, Z.Y., 2008, Eocene melting of subducting continental crust and early uplifting of central Tibet: Evidence from central-western Qiangtang high-K calc-alkaline andesites, dacites and rhyolites: Earth and Planetary Science Letters, v. 272, p. 158–171. doi:10.1016/j.epsl.2008.04.034.

Wang, Q., Wyman, D.A., Xu, J.-F., Zhao, Z.-H., Jian, P., Xiong, X.-L., Bao, Z.-W., Li, C.-F., and Bai, Z.-H., 2006a, Petrogenesis of Cretaceous adakitic and shoshonitic igneous rocks in the Luzong area, Anhui Province (eastern China): Implications for geodynamics and Cu-Au mineralization: Lithos, v. 89, p. 424–446. doi:10.1016/j.lithos.2005.12.010.

Wang, Q., Xu, J.F., Jian, P., Bao, Z.W., Zhao, Z.H., Li, C.F., Xiong, X.L., and Ma, J.L., 2006b, Petrogenesis of adakitic porphyries in an extensional tectonic setting, Dexing, South China: Implications for the genesis of porphyry copper mineralization: Journal of Petrology, v. 47, p. 119–144. doi:10.1093/petrology/egi070.

Wang, Q., Zhu, D.-C., Zhao, Z.-D., Liu, S.-A., Chung, S.-L., Li, S.-M., Liu, D., Dai, J.-G., Wang, L.-Q., and Mo, X.-X., 2014, Origin of the ca. 90Ma magnesia-rich volcanic rocks in SE Nyima, central Tibet: Products of lithospheric delamination beneath the Lhasa-Qiangtang collision zone: Lithos, v. 198–199, p. 24–37. doi:10.1016/j.lithos.2014.03.019.

Wen, D.-R., Chung, S.-L., Song, B., Iizuka, Y., Yang, H.-J., Ji, J.Q., Liu, D.Y., and Gallet, S., 2008a, Late Cretaceous Gangdese intrusions of adakitic geochemical characteristics, SE Tibet: Petrogenesis and tectonic implications: Lithos, v. 105, p. 1–11. doi:10.1016/j.lithos.2008.02.005.

Wen, D.R., Liu, D.Y., Chung, S.L., Chu, M.F., Ji, J.Q., Zhang, Q., Song, B., Lee, T.Y., Yeh, M.W., and Lo, C.H., 2008b, Zircon SHRIMP U–Pb ages of the Gangdese Batholith and implications for Neotethyan subduction in southern Tibet: Chemical Geology, v. 252, p. 191–201. doi:10.1016/j.chemgeo.2008.03.003.

Wiedenbeck, M., Alle, P., Corfu, F., Griffin, W., Meier, M., Oberli, F., Quadt, A., Roddick, J., and Spiegel, W., 1995, Three natural zircon standards for U–Th–Pb, Lu–Hf, trace element and REE analyses: Geostandards and Geoanalytical Research, v. 19, p. 1–23. doi:10.1111/j.1751-908X.1995.tb00147.x.

Wu, F.-Y., Ji, W.-Q., Liu, C.-Z., and Chung, S.-L., 2010, Detrital zircon U–Pb and Hf isotopic data from the Xigaze fore-arc basin: Constraints on Transhimalayan magmatic evolution in southern Tibet: Chemical Geology, v. 271, p. 13–25. doi:10.1016/j.chemgeo.2009.12.007.

Wu, F.-Y., Ji, W.-Q., Wang, J.-G., Liu, C.-Z., Chung, S.-L., and Clift, P.D., 2014, Zircon U–Pb and Hf isotopic constraints on the onset time of India–Asia collision: American Journal of Science, v. 314, p. 548–579. doi:10.2475/02.2014.04.

Wu, F.-Y., Yang, Y.-H., Xie, L.-W., Yang, J.-H., and Xu, P., 2006, Hf isotopic compositions of the standard zircons and baddeleyites used in U–Pb geochronology: Chemical Geology, v. 234, p. 105–126. doi:10.1016/j.chemgeo.2006.05.003.

Xie, L.W., Zhang, Y.B., Zhang, H.H., Sun, J.F., and Wu, F.Y., 2008, In situ simultaneous determination of trace elements, U–Pb and Lu–Hf isotopes in zircon and baddeleyite: Chinese Science Bulletin, v. 53, p. 1565–1573. doi:10.1007/s11434-008-0086-y.

Yin, A., and Harrison, T.M., 2000, Geologic Evolution of the Himalayan–Tibetan Orogen: Annual Review of Earth and Planetary Sciences, v. 28, p. 211–280. doi:10.1146/annurev.earth.28.1.211.

Yu, Y.S., Yang, Z.S., Duo, J., Hou, Z.Q., Tian, S.H., Meng, X.J., Liu, H.F., Zhang, J.S., Wang, H.P., and Liu, Y.C., 2011a, Age and petrogenesis of magmatic rocks from Jiaduobule skarn Fe–Cu deposit in Tibet: Evidence from zircon SHRIMP U–Pb dating, Hf isotope and REE: Mineral Deposits, v. 30, p. 420–434. [In Chinese with English Abstract.]

Zhang, G.Y., Zheng, Y.Y., Gong, F.Z., Gao, S.B., Qu, W.J., Pang, Y.C., Shi, Y.R., and Yin, S.Y., 2008, Geochronologic constraints on magmatic intrusions and mineralization of the Jiru porphyry copper deposit, Tibet associated with continent-continent collisional process: Acta Petrologica Sinica, v. 24, p. 473–479. [In Chinese with English Abstract.]

Zhang, H.F., Xu, W.C., Guo, J.Q., Zong, K.Q., Cai, H.M., and Yuan, H.L., 2007, Zircon U–Pb and Hf isotopic composition of defromed granited in the southern margin of the Gangdese belt, Tibet: Evidence for early Jurassic subduction of Neo-Tethyan oceanic slab: Acta Petrologica Sinica, v. 23, p. 1347–1353. [In Chinese with English Abstract.]

Zhang, Z.M., Zhao, G.C., Santosh, M., Wang, J.L., Dong, X., and Liou, J.G., 2010b, Two stages of granulite facies metamorphism in the eastern Himalayan syntaxis, south Tibet: Petrology, zircon geochronology and implications for the subduction of Neo-Tethys and the Indian continent beneath Asia: Journal of Metamorphic Geology, v. 28, p. 719–733.

Zhang, Z.M., Zhao, G.C., Santosh, M., Wang, J.L., Dong, X., and Shen, K., 2010a, Late Cretaceous charnockite with adakitic affinities from the Gangdese batholith, southeastern Tibet: Evidence for Neo-Tethyan mid-ocean ridge subduction?: Gondwana Research, v. 17, p. 615–631. doi:10.1016/j.gr.2009.10.007.

Zhao, J.X., Qin, K.Z., Li, G.M., Li, J.X., Xiao, B., Chen, L., Yang, Y.H., Li, C., and Liu, Y.S., 2014, Collision-related genesis of the Sharang porphyry molybdenum deposit, Tibet: Evidence from zircon U–Pb ages, Re–Os ages and Lu–Hf isotopes: Ore Geology Reviews, v. 56, p. 312–326. doi:10.1016/j.oregeorev.2013.06.005.

Zhao, Z., Hu, D.G., Lu, L., and Wu, H.Z., 2013, Discovery and metallogenic significance of the Late Cretaceous

adakites from Zetang, TIbet: Journal of Geomechanics, v. 19, p. 45–52. [In Chinese with English Abstract.]

Zheng, Y.-C., Hou, Z.-Q., Gong, Y.-L., Liang, W., Sun, Q.-Z., Zhang, S., Fu, Q., Huang, K.-X., Li, Q.-Y., and Li, W., 2014a, Petrogenesis of Cretaceous adakite-like intrusions of the Gangdese Plutonic Belt, southern Tibet: Implications for mid-ocean ridge subduction and crustal growth: Lithos, v. 190–191, p. 240–263. doi:10.1016/j.lithos.2013.12.013.

Zheng, Y.Y., Sun, X., Gao, S.B., Zhao, Z.D., Zhang, G.Y., Wu, S., You, Z.M., and Li, J.D., 2014b, Multiple mineralization events at the Jiru porphyry copper deposit, southern Tibet: Implications for Eocene and Miocene magma sources and resource potential: Journal of Asian Earth Sciences, v. 79 (Part B), p. 842–857, doi:10.1016/j.jseaes.2013.03.029.

Zhu, D.-C., Pan, G.-T., Chung, S.-L., Liao, Z.-L., Wang, L.-Q., and Li, G.-M., 2008, SHRIMP zircon age and geochemical constraints on the origin of Lower Jurassic volcanic rocks from the Yeba Formation, southern Gangdese, south Tibet: International Geology Review, v. 50, p. 442–471. doi:10.2747/0020-6814.50.5.442.

Zhu, D.-C., Zhao, Z.-D., Niu, Y.L., Dilek, Y., Hou, Z.-Q., and Mo, X.-X., 2013, The origin and pre-Cenozoic evolution of the Tibetan Plateau: Gondwana Research, v. 23, p. 1429–1454. doi:10.1016/j.gr.2012.02.002.

Zhu, D.-C., Zhao, Z.-D., Niu, Y.L., Mo, X.-X., Chung, S.-L., Hou, Z.-Q., Wang, L.-Q., and Wu, F.-Y., 2011, The Lhasa Terrane: Record of a microcontinent and its histories of drift and growth: Earth and Planetary Science Letters, v. 301, p. 241–255. doi:10.1016/j.epsl.2010.11.005.

Zhu, D.-C., Zhao, Z.-D., Pan, G.-T., Lee, H.-Y., Kang, Z.-Q., Liao, Z.-L., Wang, L.-Q., Li, G.-M., Dong, G.-C., and Liu, B., 2009, Early cretaceous subduction-related adakite-like rocks of the Gangdese Belt, southern Tibet: Products of slab melting and subsequent melt–peridotite interaction?: Journal of Asian Earth Sciences, v. 34, p. 298–309. doi:10.1016/j.jseaes.2008.05.003.